

**Steady State and Transient Response Characteristics of Commercial Non-Dispersive  
Infrared Carbon Dioxide Sensors**

by

Matthew Ian Roberts

A thesis submitted to the Graduate Faculty of  
Auburn University  
in partial fulfillment of the  
requirements for the Degree of  
Master of Science

Auburn, Alabama  
May 4, 2014

Keywords: Airline Cabin Environment Research (ACER), Carbon Dioxide,  
Non-dispersive Infrared (NDIR) Sensor, Fume Event, Bleed Air Contamination,  
Demand Control Ventilation (DCV)

Copyright 2014 by Matthew Ian Roberts

Approved by

Ruel A. Overfelt, Chair, Professor of Mechanical Engineering  
Bart Prorok, Professor of Mechanical Engineering  
Jeffrey Fergus, Professor of Mechanical Engineering

## **Abstract**

Non-dispersive infrared CO<sub>2</sub> sensors are well established and are commonly used to provide demand control ventilation for commercial buildings. The aviation industry has shown potential interest in adapting these sensors to provide air quality monitoring in airliner cabins. Two possible applications have been identified: CO<sub>2</sub> sensors have the potential to detect bleed air contamination events and provide demand control ventilation by determining the adequacy of ventilation to dissipate contaminants emitted by the passengers and materials which are present in the cabin.

To evaluate the suitability of these NDIR sensors for the two proposed applications, three commercial NDIR CO<sub>2</sub> sensors with a variety of form factors were obtained. The sensors were exposed to near instantaneous changes in CO<sub>2</sub> concentration to determine their transient and steady state responses. Because the levels of CO<sub>2</sub> are not expected to reach steady state during a transitory contamination event, it is important to understand the sensors' transient response. Therefore, this response was evaluated under two sets of conditions. In the first set of experiments, the gas was flowed through inlet and outlet ports integrated into the sensor. In the second set of experiments, the gas was allowed to diffuse into the sensor from the surrounding environment. In both cases, the sensors' readings were allowed to reach equilibrium and their steady state performances were characterized by applying a range of CO<sub>2</sub> concentrations.

## **Acknowledgements**

I would like to express sincere appreciation for my advisor, Dr. Ruel Overfelt, for his direction through my graduate education. I would also like to thank Dr. Bart Prorok and Dr. Jeffrey Fergus for their guidance and service on my committee. Additionally, I would like to thank Dr. Steve Duke for his insights during our weekly progress meetings.

I would like to recognize my fellow students who have helped tremendously with this effort. I would like to specifically mention: Amy Buck, Bethany Brooks and Naved Siddiqui with whom I had several illuminating discussions and who were always willing to help. I would like to acknowledge Vignesh Venkatasubramanian and Mobbassar Hassan Sk for their help as well. I would like to express my gratitude to those whose previous work formed the foundation of my research, John Andress and Lance Haney. I would especially like to convey my sincere appreciation to our staff physicist, Mike Crumpler, for his invaluable patience, support and technical expertise on this project.

Finally, I would like to thank my family and Caitlyn Piper for all the time spent proofreading my papers. Without their guidance and persistent help, this thesis would not have been possible.

This project was partially funded by the U.S. Federal Aviation Administration (FAA) Office of Aerospace Medicine through the National Air Transportation Center of Excellence for Research in the Intermodal Transport Environment (RITE), Cooperative

Agreement 10-C-RITE-AU. Although the FAA has sponsored this project, it neither endorses nor rejects the findings of this research.

## Table of Contents

Abstract.....	ii
Acknowledgements.....	iii
Table of Contents.....	v
List of Tables.....	viii
List of Figures.....	ix
List of Abbreviations.....	xii
List of Symbols.....	xiv
1. Introduction.....	1
2. Literature Review.....	6
2.1 Non-dispersive Infrared Sensors.....	11
2.2 Environmental Control Systems.....	13
2.3 Bleed Air Contamination.....	16
2.4 Demand Control Ventilation.....	18
3. Experimental Procedures.....	20
3.1 Commercial NDIR Sensors.....	20
3.2 Data Acquisition.....	23

3.3 Available Gas Compositions.....	24
3.4 Sensor Experiments .....	25
3.4.1 Flowing Gas Experiments.....	26
3.4.2 Elevated Temperature Tests.....	30
3.4.3 Diffusion-Based Sampling Experiments.....	31
3.4.4 Micropump Experiments .....	35
4. Results and Discussion .....	38
4.1 Steady State Results .....	38
4.1.1 Accuracy .....	38
4.1.2 Hysteresis.....	39
4.1.4 Temperature Sensitivity .....	41
4.1.3 Noise .....	47
4.2 Transient Results.....	50
4.2.1 Time to Detection .....	51
4.2.2 Response Time.....	52
4.2.2.1 Flowing Gas Experiments.....	53
4.2.2.2 Diffusion Experiments .....	57
4.2.2.3 Micropump Experiments .....	60
4.2.2.4 Baffle Experiments .....	63
5. Conclusions.....	65

6. Future Work .....	67
7. References .....	68
Appendix I: Airgas Certificates of Analysis .....	73
Appendix II: Madur madIR-DO1 CO <sub>2</sub> Certificate of Calibration .....	82
Appendix III: Accuracy Evaluation Data .....	83
Appendix IV: Effect of Flow Rate and Averaging on Response Curves .....	85

## List of Tables

Table 1: Typical interactions of electromagnetic radiation with matter [27] .....	7
Table 2: Air quality standards [9, 15, 16] .....	18
Table 3: Sensor manufacturer specifications for each evaluated sensor. [37-40].....	22
Table 4: Conversion of analogue output voltages to CO <sub>2</sub> concentrations in ppmv .....	24
Table 5: Composition of premixed gas cylinders used in this study: The CO <sub>2</sub> concentrations were balanced with N <sub>2</sub> gas.....	25
Table 6: Summary of flow rates used for the flowing gas experiments .....	28
Table 7: Summary of the accuracy of each sensor from 0 to 1889 ppmv .....	39
Table 8: Summary of RMS noise evaluation of each sensor without running average ....	49
Table 9: Summary of the noise evaluation of each sensor with a one second running average applied. ....	50
Table 10: Limits of detection for the three sensors.....	52
Table 11: Time to detection for each sensor .....	52
Table 12: Response times obtained from the flowing gas tests .....	56
Table 13: Response times of the E2V IR11EJ and Figaro K30 sensors obtained using diffusion based sampling with a difference between initial and final concentration greater than 200 ppmv. ....	59
Table 14: Response time of Figaro K30 to micropump experiments .....	62
Table 15: Response time of E2V IR11EJ to micropump experiments .....	62
Table 16: Effect of baffles on E2V IR11EJ response times .....	64



## List of Figures

Figure 1: Schematic of a typical bleed air system [6].....	2
Figure 2: Energy diagram showing rotational, vibrational and electronic States [7] .....	7
Figure 3: IR vibrational modes [28].....	8
Figure 4: Infrared absorbance spectra of CO <sub>2</sub> from QASoft® database [7] .....	9
Figure 5: First fundamental vibrational mode of CO <sub>2</sub> , symmetric stretching, .....	9
Figure 6: Second fundamental vibrational mode of CO <sub>2</sub> , bending,.....	10
Figure 7: Third fundamental vibrational mode of CO <sub>2</sub> , asymmetric stretching,.....	10
Figure 8: Schematic of a typical NDIR Sensor.....	11
Figure 9: Schematic of a typical airliner bleed air system [2] .....	14
Figure 10: Comparison of air exchange rates in various environments [4].....	16
Figure 11: Sensors and evaluation boards investigated: Madur madIR-DO1 CO <sub>2</sub> , E2V IR11EJ, Figaro K30 .....	22
Figure 12: The desired CO <sub>2</sub> concentration profile (dashed line) compared to the expected sensor response (solid line).....	26
Figure 13: Block diagram of flowing gas apparatus with inlay showing the gassing hood on the E2V IR11EJ. ....	27
Figure 14: Response time of hooded E2V IR11EJ to 1899 ppmv CO <sub>2</sub> as a function of volumetric flow rate .....	29
Figure 15: Schematic of the apparatus used to control the temperature of flowing gas ...	31
Figure 16: Block diagram of diffusion testing apparatus used with Figaro K30 and E2V IR11EJ sensors.....	33
Figure 17: Chamber used to test diffusion-based sampling of Figaro K30 and E2V IR11EJ sensors.....	33

Figure 18: Schematic of the apparatus used to create diluted gas concentrations. A micropump is used to pump the diluted gas into the sensor. ....	36
Figure 19: Parker Fluidics H022C-11 diaphragm pump used to provide gas to the E2V IR11EJ while conducting micropump experiments with a dime shown for size comparison.....	37
Figure 20: Measured reading of each sensor compared to the concentration of a set of known gasses. The dashed line indicates the ideal 1:1 ratio and the dotted bands indicate the analytical uncertainty of the known gas concentrations. ..	39
Figure 21: Concentration profile used to conduct a hysteresis evaluation on each sensor. ....	40
Figure 22: Measured CO <sub>2</sub> concentration of Madur madIR-D01 CO <sub>2</sub> during hysteresis test. The results are typical of all sensors tested showing no hysteresis loop. ....	41
Figure 23: Chart showing steady state measurements recorded by the Madur madIR-D01 CO <sub>2</sub> at various temperatures to known gas concentrations before applying ideal gas law calibration.....	44
Figure 24: Chart showing the steady state measurements recorded by the Madur madIR-D01 at various temperatures to known gas concentrations after applying the ideal gas law calibration.....	44
Figure 25: Steady state measurements recorded by the Figaro K30 at various temperatures to known gas concentrations .....	46
Figure 26: Steady state measurements recorded by the E2V IR11EJ at various temperatures to known gas concentrations .....	46
Figure 27: Response of the Figaro K30 sensor a flowing gas experiment illustrating the both stepwise response and noise present in the signal. The concentration was changed from 400 ppmv to a 797.1 ppmv near instantaneously when the time was equal to zero.....	48
Figure 28: Response of the Figaro K30 sensor to a flowing gas experiment illustrating the two transient parameters: time to detection and response time. The concentration was changed from 400 ppmv to a 797.1 ppmv near instantaneously when the time was equal to zero. ....	51
Figure 29: Normalized response of the Madur madIR-D01 CO <sub>2</sub> sensor to the flowing gas experiments. The concentration was changed from 400 ppmv to a variety of concentrations near instantaneously when the time was equal to zero. ....	54
Figure 30: Normalized Response of the E2V IR11EJ sensor to the flowing gas experiments. The concentration was changed from 400 ppmv to a variety of concentrations near instantaneously when the time was equal to zero. ....	55

Figure 31: Normalized Response of the Figaro K30 sensor to the flowing gas experiments. The concentration was changed from 400 ppmv to a variety of concentrations near instantaneously when the time was equal to zero. .... 56

Figure 32: Comparison of the normalized response of three sensors to flowing gas experiment. The concentration was changed from 400 ppmv to 1889 ppmv near instantaneously when the time was equal to zero. .... 57

Figure 33: Response time of E2V IR11EJ employing diffusion based sampling as a function of concentration difference between initial and final concentrations. .... 58

Figure 34: Response time of Figaro K30 employing diffusion based sampling as a function of concentration difference between initial and final concentrations. .... 58

Figure 35: Normalized Response of the E2V IR11EJ and Figaro K30 sensor to the diffusion experiments. The concentration was changed from 554.71 ppmv to 1081.78 near instantaneously when the time was equal to zero. .... 60

Figure 36: Comparison of flowing gas tests with and without baffle incorporated in the gassing hood..... 63

## **List of Abbreviations**

AIDS	Accident and Incident Data System
ASHRAE	American Society of Heating, Refrigerating and Air Conditioning Engineers
CO	Carbon Monoxide
CO <sub>2</sub>	Carbon Dioxide
DAC	Digital to Analogue Converter
DCV	Demand Control Ventilation
ECS	Environmental Control System
EPA	Environmental Protection Agency
FAA	Federal Aviation Administration
HEPA	High Efficiency Particulate Air
HVAC	Heating, Ventilation, and Air-Conditioning
Hz	Hertz
IC	Integrated Circuit
N <sub>2</sub>	Molecular Nitrogen Gas
NASA	National Aeronautics and Space Administration
NDIR	Non-Dispersive Infrared
O <sub>2</sub>	Molecular Oxygen Gas
OSHA	Occupational Safety and Health Administration

PPMV	Parts Per Million by Volume
PSIA	Pounds per Square Inch Absolute
PSIG	Pounds per Square Inch Gauge
PVC	Polyvinyl Chloride
RMS	Root Mean Square
SDR	Service Difficulties Reports
USB	Universal Serial Bus
VDC	Volts Direct Current
VIPR	Vehicle Integrated Propulsion Research

## List of Symbols

$\varepsilon$	Molar absorption coefficient
$\tau$	Time constant
$A$	Cross sectional area
$C$	CO <sub>2</sub> concentration
$C_{\text{Equivalent}}$	Equivalent concentration at the calibrated temperature and pressure
$C_{\text{Final}}$	Concentration in the chamber after the test gas is introduced
$C_{\text{Initial}}$	CO <sub>2</sub> concentration of the gas in the chamber prior to test
$C_{\text{Measured}}$	Concentration as measured by a NDIR sensor
$C_{\text{Test Gas}}$	Concentration of the premixed gas
$E$	Voltage
$I$	Intensity of the infrared radiation in the presence of the target gas
$I_0$	Intensity of the infrared radiation in the absence of the target gas
$l$	Path length of the NDIR Sensor
$N$	Number of readings
$P$	Absolute pressure
$P_{\text{cal}}$	Absolute pressure at which the sensor was calibrated
$Q$	Volumetric flow rate

$T$	Absolute temperature
$T_{\text{Cal}}$	Absolute temperature at which the sensor was calibrated
$V$	Volume
$V_{\text{Test Gas}}$	Volume of premixed gas introduced to chamber
$V_{\text{Chamber}}$	Volume of the diffusion chamber
$\bar{x}$	Average sensor reading
$x_i$	A given sensor reading
$x_{RMS}$	Root mean square noise

## **1. Introduction**

Non-dispersive infrared (NDIR) sensors are the most commonly employed method to measure the concentration of carbon dioxide (CO<sub>2</sub>). For years, these sensors have been used successfully in commercial buildings to provide demand control ventilation. The purpose of this study is to characterize the steady state and transient response of three commercial NDIR sensors to determine if they are suitable for aviation air-quality applications. Two potential uses have been identified: monitoring the bleed air system to detect fume events and providing demand control ventilation onboard aircraft.

Commercial aircraft routinely operate at cruising altitudes of up to 41,000 feet. At this elevation, the outside pressure is less than 2.9 psia and the temperature can drop to below -70°F (-57 °C) [1-3]. Under these conditions, humans cannot survive unaided. Consequently, airliners are equipped with an environmental control system (ECS) which provides for the safety and comfort of passengers by pressurizing the cabin with clean, temperature controlled air. In most commercial airliners, the cabin air is supplied by a bleed air system (Figure 1). This system “bleeds off” a portion of the air passing through the compressor stage of the engine. The air from the compressor is then cooled by heat exchangers and air conditioning packs before being combined with HEPA filtered, recirculated cabin air in the mixing unit and distributed throughout the cabin [2-5].



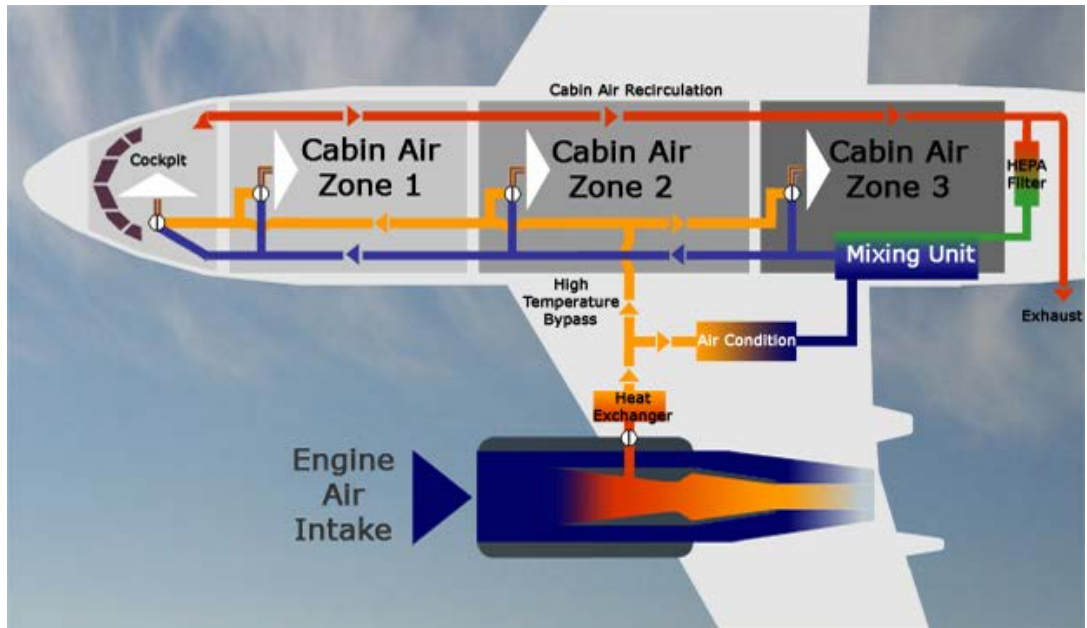


**Figure 1:** Schematic of a typical bleed air system [6]

Usually, the environmental control system works as intended and provides a clean conditioned environment in the aircraft cabin. However, the cabin air can be degraded if the bleed air becomes contaminated or if the cabin ventilation is insufficient to dissipate contaminants released by the occupants and materials present in the cabin [7-14]. To ensure the cabin environment remains safe and comfortable, the FAA has set acceptable limits of various contaminants such as CO, CO<sub>2</sub>, ozone and particulate matter; however, these regulations currently do not require onboard monitoring [9, 15, 16]. This study evaluates the possibility that NDIR CO<sub>2</sub> sensors could be used to partially fulfill this monitoring role.

On occasion, there are incidents where the bleed air system provides contaminated air to the passenger cabin. These events are believed to be caused by oil and hydraulic fluid leaking from seals or de-icing fluid being accidentally introduced into the engine [7-11].

Additionally, contaminants which are present in the surrounding air can be introduced to the bleed air system. The airplane's jet engine can ingest exhaust from ground equipment or nearby aircraft [17]. At altitude, the airplane can ingest ozone which is present in the upper atmosphere [2, 4, 17]. Since the contaminant levels are unlikely to reach steady state in a transitory contamination event, it is important to examine the transient response of any sensors which may be used to monitor these events.

There is disagreement in the literature concerning the frequency of these events. During 2012 in the United States, there was an average of 23,419 flights per day [18]. Therefore, according to various studies, the frequency of contamination events could range from 0.70 to 234 flights per day. Murawski and Supplee conducted a study which examined the Accident and Incident Data System (AIDS) and Service Difficulty Reports (SDR) maintained by the FAA for keywords related to fume events over an 18 month period from January 2006 to June 2007. The study concluded that 0.86 contamination events per day occurred [19]. During this period, there was an average of 28,949 flights per day [18], and this corresponds to a rate of incidence of 0.003 % of flights. The British Committee on Toxicology estimated that 1 % of flights were contaminated based on pilot reports; however, the committee found a much lower contamination occurrence, 0.05 % of flights, when only maintenance reports were considered [20, 21].

The second proposed application of NDIR sensors is to provide demand control ventilation. The contamination originating in the bleed air system is not the only source of contamination in an aircraft cabin; the majority of contaminants are produced by the occupants themselves who emit CO<sub>2</sub>, body odors, and microbial aerosols [4]. Currently, airplanes are designed to constantly provide a fixed percentage of fresh air, enough to

dissipate these contaminants when the plane is at full capacity; however, the occupancy of the air plane fluctuates [4]. It is theorized that the efficiency of the airplane could be increased if the amount of fresh air provided by the bleed air system engine could be modulated based on actual occupancy. In periods of decreased occupancy, more air could be recirculated. Less fresh air would be required to ventilate the cabin sufficiently to remove contaminants emitted by passengers.

NDIR CO<sub>2</sub> sensors are already common in demand control ventilation systems present in commercial buildings [22]. The sensors are used to provide an indication of building occupancy and determine required ventilation levels. The sensor readings are used as a surrogate to determine the adequacy of ventilation to remove contaminants released by the occupants and building materials. At the levels found in buildings and airplanes, CO<sub>2</sub> itself does not provide a health hazard; however, buildup of CO<sub>2</sub> coincides with the accumulation of other contaminants released by the occupants [22-24]. The ASHRAE building standards stipulate that the difference between indoor and outdoor CO<sub>2</sub> concentrations remains less than 700 ppmv to ensure the comfort of the occupant based on odor levels [25]. However, a different value would be needed for aircraft which have enhanced exchange rates and filtering capabilities [4].

To evaluate the suitability of these NDIR sensors for the two proposed applications, three commercial NDIR CO<sub>2</sub> sensors with a variety of form factors were obtained. The sensors were exposed to near instantaneous changes in CO<sub>2</sub> concentration, and their transient responses were determined. This transient response was evaluated under two sets of conditions. In the first set of experiments, the gas was passed through inlet and outlet ports integrated into the sensor. In the second set of experiments, the changed gas

concentration was allowed to diffuse into the sensor from the surrounding environment. In both cases, the sensors' readings were allowed to reach equilibrium and their steady state performances were characterized by applying a range of CO<sub>2</sub> concentrations.

## 2. Literature Review

### Infrared Spectrum

If a photon of light has the proper energy, it can be absorbed by a gas molecule causing the gas molecule to transition to a higher energy state. The energy of the photon must be equal to the energy difference between two energy levels of the molecule. These energy states can arise from changes in molecular rotation, vibration, and electronic transitions [26]. Of these three changes, the electronic transitions require the most energy and tend to occur in the visible and ultraviolet range. Changes in the vibrational state of a molecule require less energy and occur at shorter wavelengths in the infrared range. Molecular rotations require the least energy and occur in the microwave range [27]. Table 1 summarizes typical interactions of electromagnetic radiation with matter. The information is presented in terms of wavelength and its reciprocal, wavenumber, which is the unit commonly used in spectroscopy.

**Table 1:** Typical interactions of electromagnetic radiation with matter [27]

	Visible & Ultraviolet	Near Infrared	Mid-Infrared	Far Infrared	Microwaves
<b>Wavelength</b>	$1 \times 10^{-8} m$ to $7 \times 10^{-7} m$	$7 \times 10^{-7} m$ to $2.5 \times 10^{-6} m$	$2.5 \times 10^{-6} m$ to $2.5 \times 10^{-5} m$	$2.5 \times 10^{-6} m$ to $2.5 \times 10^{-3} m$	$2.5 \times 10^{-3} m$ to $1 m$
<b>Wavenumber</b>	$1,000,000 \text{ cm}^{-1}$ to $14,000 \text{ cm}^{-1}$	$14,000 \text{ cm}^{-1}$ to $4000 \text{ cm}^{-1}$	$4000 \text{ cm}^{-1}$ to $400 \text{ cm}^{-1}$	$400 \text{ cm}^{-1}$ to $4 \text{ cm}^{-1}$	$4 \text{ cm}^{-1}$ to $0.01 \text{ cm}^{-1}$
<b>Interaction</b>	Electronic Transitions	Molecular Vibrations	Molecular Vibrations	Molecular Vibrations	Molecular Rotations

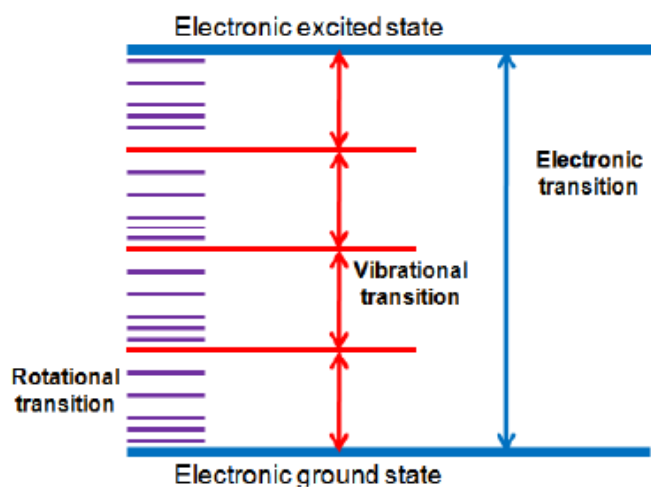


**Figure 2:** Energy diagram showing rotational, vibrational and electronic states [7]

Infrared absorption spectra are the result of atomic nuclei vibrating periodically within molecules. Each type of molecular vibration absorbs energy at specific wavelengths which are determined based on the symmetry and types of bonds present in the molecule. Every atom in a molecule can move in three directions (x,y,z), so a molecule comprised of N atoms has 3N degrees of freedom. The entire molecule can translate in or rotate around the three axes. These types of motion are non-vibrational,

and by eliminating them it can be shown that there are up to  $3N-6$  vibrational modes or  $3N-5$  vibrational modes in linear molecules. These vibrations are commonly classified into categories, which include two stretching modes: symmetric stretch, asymmetric stretch and four bending modes: scissoring, rocking, wagging and twisting [26].

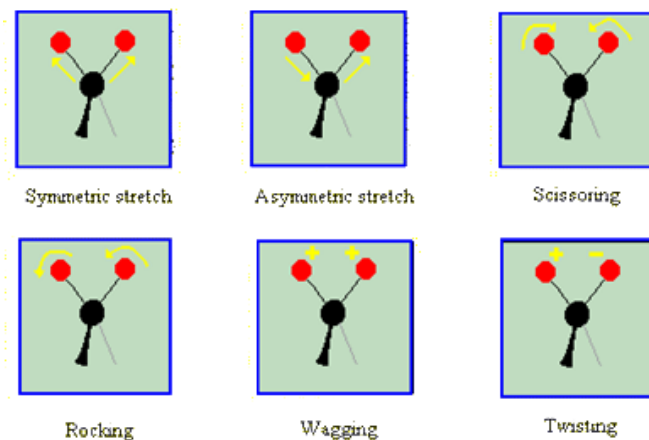


**Figure 3:** IR vibrational modes [28]

The absorption of energy at wavelengths which correspond to each vibrational mode gives rise to the infrared absorption spectrum of a sample. Since carbon dioxide is a linear molecule consisting of three atoms, it has four modes of vibration. However, the infrared spectrum of carbon dioxide shows only two distinct peaks. One of the degrees of freedom is inactive in the infrared and two of the modes are degenerate.

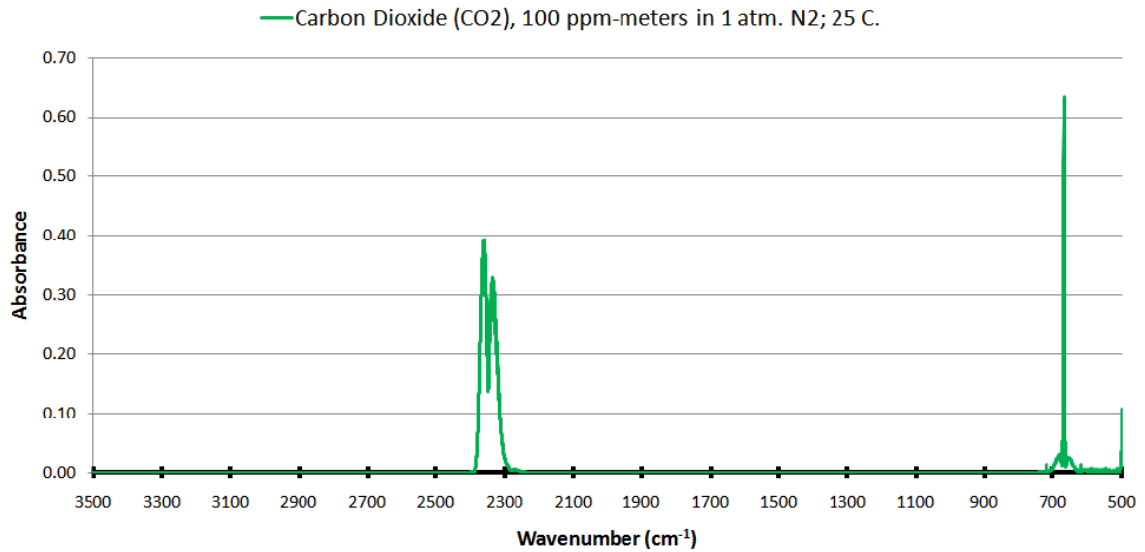


**Figure 4:** Infrared absorbance spectra of CO<sub>2</sub> from QASoft® database [7]

The first vibrational mode occurs at  $1340\text{ cm}^{-1}$ . The oxygen-carbon bonds stretch symmetrically and the carbon atom is fixed. This mode is inactive in the infrared because there is not a change in the dipole moment.

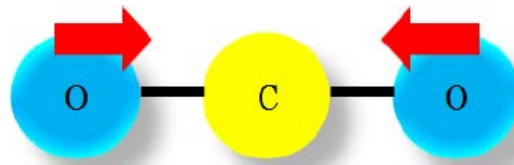


**Figure 5:** First fundamental vibrational mode of CO<sub>2</sub>, symmetric stretching,

$$k_1=1340\text{ cm}^{-1}, \lambda_1=7.46\text{ }\mu\text{m [7]}$$

The second fundamental vibrational mode is the bending mode; the oxygen atoms oscillate in an antiparallel direction from the carbon. There are two degenerate bending



modes, in-plane and out-of-plane, which are  $90^\circ$  rotations of each other and share an absorption peak at  $667\text{ cm}^{-1}$ .

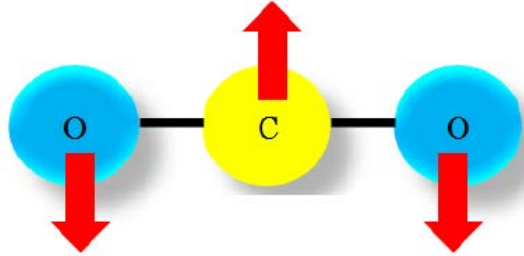


**Figure 6:** Second fundamental vibrational mode of  $\text{CO}_2$ , bending,

$$k_2=667\text{ cm}^{-1}, \lambda_2=15.0\text{ }\mu\text{m [7]}$$

The third fundamental vibrational mode is asymmetric stretching; the carbon atom moves relative to the center of mass of the two oxygen atoms. This creates an absorption peak at  $2350\text{ cm}^{-1}$  [7, 29].

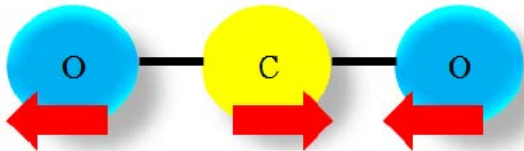


**Figure 7:** Third fundamental vibrational mode of  $\text{CO}_2$ , asymmetric stretching,

$$k_3=2350\text{ cm}^{-1}, \lambda_3=4.26\text{ }\mu\text{m [7]}$$

## 2.1 Non-dispersive Infrared Sensors

Non-dispersive infrared (NDIR) sensors as shown schematically in Figure 8 measure the concentration of a target gas, such as carbon dioxide in the present investigation, based on the absorption of infrared radiation through a gas mixture. A light source produces broad-band infrared radiation which is passed through the gas sample. Based on the molecular structure of the gas particles, these molecules will vibrate and absorb infrared energy at specific wavelengths. Carbon dioxide has a strong absorption band at  $2350\text{ cm}^{-1}$  ( $4.26\text{ }\mu\text{m}$ ) and there is very little cross sensitivity to other gases at this wavelength. The infrared radiation then strikes a detector which measures the intensity of the incoming infrared radiation. By placing a band pass filter in front of the detector, the radiation measured by the detector can be limited to a wavelength absorbed by the target gas [30, 31].

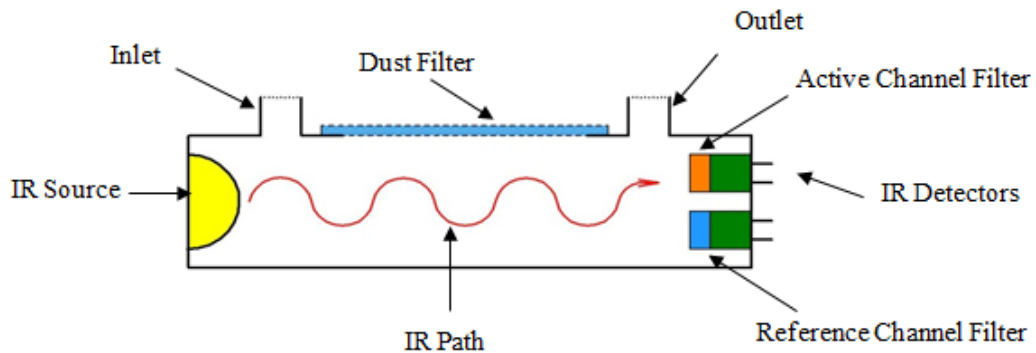


**Figure 8:** Schematic of a typical NDIR sensor

From the measured intensity, the molar concentration of the target gas can be determined using Beer-Lambert's Law (Eq. 1). The more target molecules which are present in the path length, the more infrared energy will be absorbed. In the following

equation,  $A$  is the absorbance.  $I$  and  $I_0$  represent the intensities of the infrared energy striking the detector in the presence of and absence of the target gas, respectively. The extinction coefficient, also known as molar absorptivity, is represented by  $\epsilon$  and the path length is  $l$ . The molar concentration ( $\frac{mols}{m^3}$ ) is represented by  $c$  [30, 31].

$$A = \log_{10} \frac{I_0}{I} = \epsilon cl \quad \text{Eq. 1}$$

Over time, the intensity of the infrared radiation reaching the detectors may diminish due to lamp aging or dust accumulation on the windows. To correct for this long term change and induced sensor drift, some sensors employ a dual wavelength technique involving a reference channel. The reference channel consists of another filter and detector monitoring a second wavelength not absorbed by the target gas. This reference channel allows the intensity of the lamp and window fouling to be monitored over time [31, 32].

Another method which is used to account for drift is automatic background calibration. Sensors which use this method attempt to match the lowest concentration recorded over a given interval to the ambient environmental concentration of CO<sub>2</sub> - approximately 400 ppmv. The problem with this calibration method is that it requires that the CO<sub>2</sub> concentration measured by a sensor to periodically drop to a known level. Consequently, this compensation scheme works in situations such as office buildings which are unoccupied at night during which the CO<sub>2</sub> concentration drops to outdoor

levels (i.e., 400 ppmv). In different situations, other compensation techniques such as a reference channel should be employed [31, 32].

## **2.2 Environmental Control Systems**

Commercial aircraft routinely operate at cruising altitudes of up to 41,000 feet. At this elevation, the outside pressure is less than 2.9 psia and the temperature can drop to below  $-70^{\circ}\text{F}$  ( $-57^{\circ}\text{C}$ ) [1, 2]. Under these conditions humans cannot survive unaided. At altitude, the percentage of oxygen is the same as on the ground, approximately 21%. However, the partial pressure of oxygen is lower, and this limits the binding of oxygen to hemoglobin in the blood stream [3, 8, 33]. Consequently, airliners are equipped with an environmental control system (ECS) which provides for the safety and comfort of passengers by pressurizing the cabin with clean, temperature controlled air [2, 4, 5]. The FAA mandates that the cabin be maintained at pressure greater or equal to 8000 feet above sea level, 10.9 psia [34].

The majority of airliners, with the exception of the Boeing 787, provide air to the passenger compartment using a bleed air system [6]. The bleed air system diverts a portion of the air passing through the compressor stage of the jet turbine engine used for aircraft propulsion and power. Air is extracted from a high pressure port when the engine is at low power and a low pressure port when the engine is at high power. Once the air is extracted, the bleed air temperature can reach as high as  $350^{\circ}\text{F}$  ( $177^{\circ}\text{C}$ ) and the pressure will be between 30 and 175 psia depending on the current engine settings and environmental conditions [2, 9, 10].

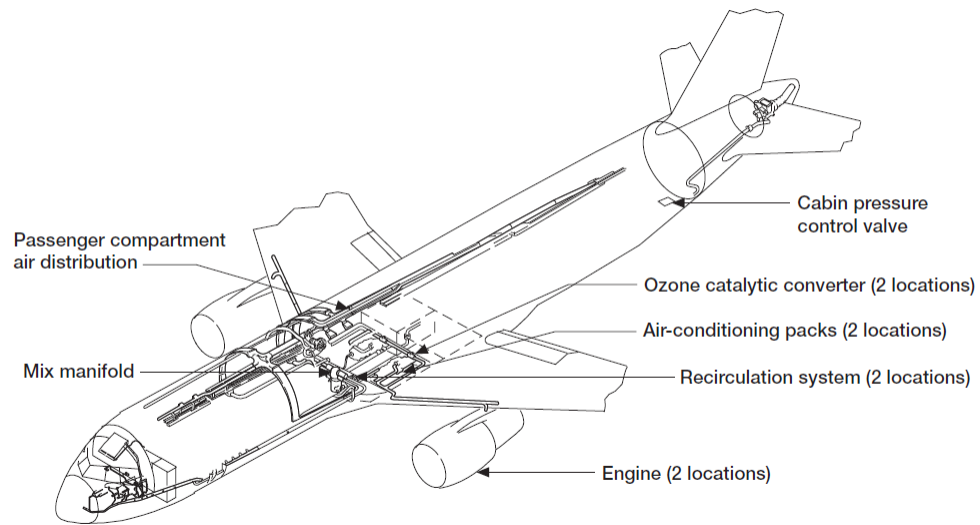


**Figure 9:** Schematic of a typical airliner bleed air system [2]

Next, the air is passed through ozone converters which catalyze the dissociation of ozone into molecular oxygen. Ozone is created by the conversion of oxygen by ultraviolet radiation, and at cruising altitudes, ozone concentrations can reach as high as 0.8 ppmv. Ozone concentrations are highest on routes at high latitude and high altitude routes during spring [2, 4, 5]. If this concentration were allowed to reach the cabin passengers could experience: shortness of breath, coughing, chest pain, eye irritation, nasal congestion, headaches and fatigue. To prevent these symptoms, ozone converters are installed which can remove 60-95% percent of the ozone from the air stream depending on how efficiently the converter's catalyst is functioning [2, 5].

The bleed air from the ozone converter is still hot; consequently, the air is passed through heat exchangers and air conditioning packs cool the air. The cooled air from the engine is then sent to a mixing manifold where it is combined with an equal amount of filtered recirculated air from the cabin. High-efficiency particulate air (HEPA) filters are

installed on airliners to remove particulates and prevent the spread of disease. These filters purify the recirculated cabin air before it is introduced into the mixing manifold [2, 4, 5]. HEPA-filters can remove particles as small as 0.003 microns with greater than 99.9% efficiency. This includes bacteria which are larger than one micron and viruses which range from .003 to 0.5 microns. Similar filters are used in critical ward of hospitals and clean rooms [2, 4].

The cooled, filtered air from the mixing manifold is then sent to an overhead distribution network which supplies air to the passengers and crew. Small amounts of hot air are added to this network to regulate the air temperature between 65 °F and 85 °F (18-29 °C). This hot air is drawn from a high temperature bypass line which circumvents the air-conditioning packs and mixing manifold. Enough fresh air is supplied to completely exchange the cabin air ten to fifteen times per hour. This exchange rate is higher than that seen in typical building (Figure 9). An airliner operates in an extreme environment and is more densely occupied. Therefore, more exchanges are necessary to provide temperature control and remove contaminants emitted by the occupants, such as CO<sub>2</sub>, body odor and microbial aerosols [2].

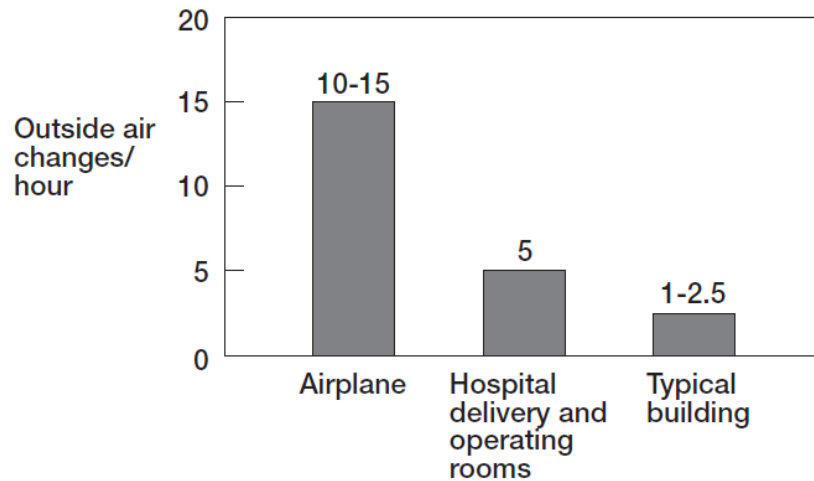


**Figure 10:** Comparison of air exchange rates in various environments [4]

### 2.3 Bleed Air Contamination

In the majority of flights, the bleed air system works as intended. However, there is the potential that contaminants could develop and reach the cabin air creating a situation known as a fume event. There are several potential sources of contamination. Oil and hydraulic fluid can leak from seals and de-icing fluid can be accidentally be introduced into the engine. Once such working fluids enter the bleed air system, they will degrade under the elevated temperatures. As they degrade, the substances have the potential to generate CO, CO<sub>2</sub>, VOCs and particulate matter [7-11]. Additionally, contaminants which are present in the surrounding air can be introduced to the bleed air system. The airplane's jet engine can ingest exhaust from ground equipment or nearby aircraft, and at altitude the airplane can ingest ozone which is present in the upper atmosphere [17].

These fume events have the potential for significant effects on the safety and health of the passengers and crew. In December 2008, an event occurred when an Alaskan Airlines

cabin was contaminated with fumes from a de-icing operation. The victims reported nausea, dizziness and eye irritation. Seven crew members were sent to the hospital and several passengers were treated on site [12]. Several fume events have been attributed to oil contamination of the bleed air system [10, 13, 14]. On one occasion, which occurred in February 2012, fumes entered the cockpit of an Air Berlin flight cabin. The co-pilot was overcome by nausea and was forced to leave the flight deck for the lavatory. He recovered in flight after being administered oxygen for fifteen minutes. Upon landing, tri-ortho-cresyl phosphate, a neurotoxin and wear additive found in engine oil was detected in his blood stream [14].

To protect the comfort and safety of those onboard commercial aircraft, the FAA has established regulations setting allowable limits for several potential contaminants. Table 2 summarizes the FAA air quality standards and compares them with the allowed limits established by other regulatory bodies. The relevant regulation 14 C.F.R. §25.831 requires that “(The) crew and passenger compartment air must be free from harmful or hazardous concentrations of gases or vapors.” The regulation further stipulates that the carbon dioxide levels must not exceed a sea level equivalent of 5,000 ppmv. However, the FAA does not stipulate how the requirements are to be met or require that the contaminate concentrations be monitored.



**Table 2:** Air quality standards [9, 15, 16]

<b>Contaminant</b>	<b>EPA (Environmental)</b>	<b>OSHA (Workplace)</b>	<b>FAA (Aircraft)</b>
<b>Carbon Monoxide</b>	35 ppmv for 1-hr. 9 ppmv for 8-hr.	50 ppmv	50 ppmv <sup>#</sup>
<b>Carbon Dioxide</b>	N/A	5000 ppmv	5000 ppmv <sup>#</sup>
<b>Particulate Matter 10 µm</b>	150 µg/m <sup>3</sup>	N/A	N/A
<b>Particulate Matter 2.5 µm</b>	65 µg/m <sup>3</sup>	N/A	N/A
<b>Ozone</b>	0.12 ppmv for 1-hr. 0.08 ppmv for 8-hr.	0.1 ppmv	0.1 ppmv <sup>*</sup> 0.25 ppmv <sup>**</sup>

<sup>#</sup> Sea level equivalent, absolute maximum -14 CFR 25.831

<sup>\*</sup> Sea level equivalent, time weighted average over a three hour interval – 14 CFR 25.832

<sup>\*\*</sup> Sea level equivalent, time weighted average over a three hour interval while above 32,000 feet -14 CFR 25.832

## **2.4 Demand Control Ventilation**

Traditionally, the quantity of fresh air supplied to a building by its HVAC system is determined by supplying a set amount of air specified in cubic feet per minute per person based on its maximum design occupancy. Demand control ventilation (DCV) is an alternative arrangement in which the amount of ventilation provided by an HVAC system is dynamically regulated by demand. The system will provide more fresh air during periods of high occupancy. Conversely, it will reduce the quantity of outside supply air (OSA) during periods of low occupancy. Outside supply air requires more energy to condition compared to recirculated air. Consequently, increased efficiency and cost savings can be obtained by, reducing the supply of OSA based on demand compared to using a set OSA flow rate during all hours of occupancy [22, 23]. Studies have shown this can result in energy savings in excess of 20% [35, 36].

NDIR CO<sub>2</sub> sensors are the industry standard for use in demand control ventilation of commercial buildings [22]. They are used to provide an indication of building occupancy and determine required ventilation levels. At the levels found in buildings, 400 to 2000 ppmv CO<sub>2</sub> itself does not create a health hazard; however, buildup of CO<sub>2</sub> coincides with the accumulation of other contaminants released by the occupants and building materials. Therefore, the sensor readings are used as a surrogate to determine the adequacy of ventilation to remove contaminants released in occupied structures [22-24]. The ASHRAE building standards stipulate that the difference in CO<sub>2</sub> concentration between indoor and outdoor air not exceed 700 ppmv to ensure the comfort of the occupant based on odor levels [25].

### **3. Experimental Procedures**

#### **3.1 Commercial NDIR Sensors**

Three inexpensive commercial non-dispersive infrared sensors were evaluated to determine their response characteristics. These sensors were selected to allow a variety of form factors and measurement methods. The Madur madIR-DO1 CO<sub>2</sub> and Figaro K30 employ a single wavelength technique and have the option to perform automatic background calibrations; although for this study, the automatic background feature was disabled. The feature was disabled because it is impossible to ensure that an airliner will experience unoccupied periods required for the automatic background feature to work properly. The third sensor, the E2V IR11EJ, is a dual wavelength sensor incorporating a reference channel. A summary of the manufacturer specifications for each sensor is shown in Table 3.

To measure the concentration of carbon dioxide in a gas sample, the gas must be introduced into the sensor. Two different methods were used to accomplish this. In some sensor designs, the gas sample flows into the sensor through an inlet port. In other sensor designs, the gas sample is allowed to simply diffuse through a dust filter into the sensing chamber. Of the sensors tested, the Madur madIR-D01 CO<sub>2</sub> sensor incorporates a micropump to move the sample gas directly through ports into the sensing chamber. The E2V IR11EJ sensor operates by allowing gas to diffuse through a dust filter into the sensing chamber. The Figaro K30 sensor allows either method to be used and

incorporates both a permeable dust filter and inlet/outlet ports. These sensors are shown below in Figure 11.

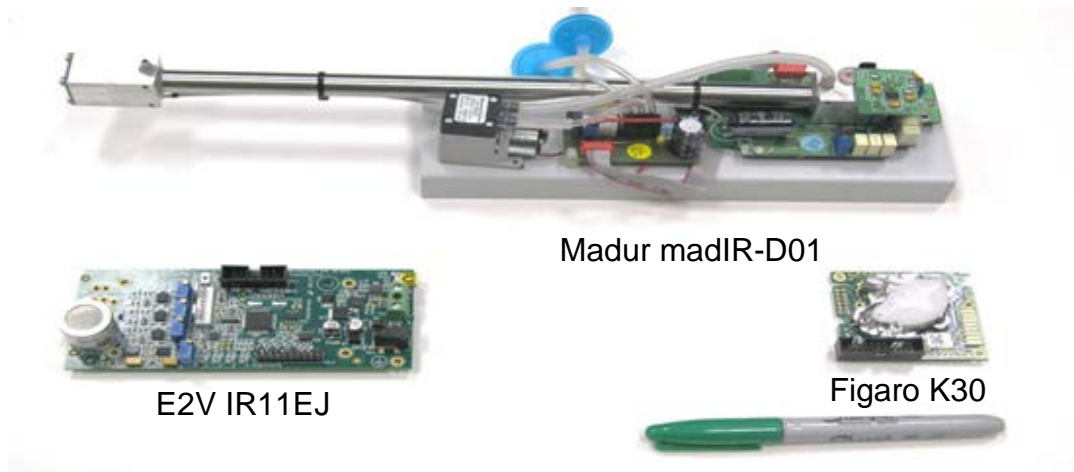


**Figure 11:** Sensors and evaluation boards investigated: Madur madIR-DO1 CO<sub>2</sub>, E2V IR11EJ, Figaro K30

**Table 3:** Sensor manufacturer specifications for each evaluated sensor. [37-40]

Model:	MADUR madIR-D01	E2V IR11EJ	Figaro K30
<b>Range:</b>	0-2500 ppmv	0 -5000 ppmv	0-2000 ppmv
<b>Resolution</b>	<1/3 Range: 1 ppmv >1/3 Range: 10 ppmv	Typical: 30 ppmv	5 mV (5 ppmv)
<b>Accuracy</b>	± (3 % of reading + 1.5 % of range)	Not Specified	±30ppm ±3% of measured ppmv
<b>Response Time:</b>	<15 sec	T <sub>90</sub> <25 sec	T <sub>1/e</sub> <20 sec
<b>Weight:</b>	220 g	Sensor: 24 g Board: 42 g	15 g*
<b>Dimensions:</b>	120 x 80 x 55 mm	Sensor: 20 Ø X 23.6mm Board: 130 x 55 mm	57.15 X 50.8 X 12.5 mm
<b>Power Requirement</b>	13-30 VDC, 165 mA	Sensor: 3-15 VDC, 60 mA Board: 9 VDC, 140 mA*	4.5-14 VDC, 40 mA
<b>Technology:</b>	Single Wavelength	Dual Wavelength	Single Wavelength
<b>Sampling Method</b>	Inlet/Outlet	Diffusion	Diffusion or Inlet/Outlet

\* Measured value which was not provided in manufacturer's datasheet.

### 3.2 Data Acquisition

The Madur madIR-D01 CO<sub>2</sub> sensor incorporates built-in electronics to process the signal from the detector and convert the signal into a concentration in ppmv. This same sensor has the capability to transmit and receive data through a RS-232 serial port. Using this port and the Mamos III v. 10.6.9 software provided by the manufacturer, the CO<sub>2</sub> concentration can be recorded and the sensor settings may be altered. The sensor can also output analogue voltage or current with the output parameters being set using the Mamos software. For this study, the voltage output was set to be from 0 to 10 VDC, corresponding linearly to concentrations ranging from 0 to 2500 ppmv.

The Figaro K30 sensor also has built-in signal processing. The sensor has the capability to transmit and receive data through a serial port using the Modbus protocol and provides an analogue voltage signal. This output range has selectable lower limits of 0, 1 or 2 VDC which the user combines with one of three upper limits: 4, 5 or 10 VDC. For this study, the sensor was left in its default configuration, i.e., an output of 0-4 VDC corresponding linearly to concentrations ranging from 0 to 2000 ppmv.

The E2V IR11EJ was paired with the IR-EK2 Evaluation Board which provided similar signal processing capabilities. With this evaluation kit, the E2V IR11EJ sensor is capable of communicating across USB. Then using the software provided with the evaluation kit, an operator can record the sensor readings and alter the sensor parameters. Before the system will operate properly, the manufacturer requires that the user first calibrate the sensor/evaluation board pair. The sensor must be exposed to a clean, dry gas, free of CO<sub>2</sub> and then a gas of a known CO<sub>2</sub> concentration (“span” gas). Pure research grade nitrogen was used as the zero gas and 1889 ppmv CO<sub>2</sub> balanced with nitrogen was

used as the span gas. The sensor can be configured to provide an analogue voltage output. The output ranged from 0 to 2.048 VDC and corresponds linearly to concentrations ranging from 0 ppmv to that of the span gas used in the calibration process.

In this study, the concentrations were recorded using each sensor’s analogue output. Table 4 summaries the equations used to convert the analogue output voltage (E) into a CO<sub>2</sub> concentration in ppmv. The analogue signals were passed to a four-channel DI-158 USB data acquisition module produced by Dataq Instruments, Akron, OH. This module was set to sample at the maximum rate, 240 Hz. However, this sampling rate is split evenly between all the active channels; therefore, the acquisition rate for each channel was 60 Hz. The files were saved as a comma separated value (.csv) file for further analysis in a custom-built Matlab program.

**Table 4:** Conversion of analogue output voltages to CO<sub>2</sub> concentrations in ppmv

Sensor	Output Range	Concentration Range	Conversion Equation
Madur madIR-D01	0.0 to 10.0 VDC	0-2500 ppmv	$C_{\text{ppmv}} = 250 \frac{\text{ppmv}}{\text{volt}} \cdot E$
Figaro K30	0.0 to 4.0 VDC	0-2000 ppmv	$C_{\text{ppmv}} = 500 \frac{\text{ppmv}}{\text{volt}} \cdot E$
E2V IR11EJ	0.0 to 2.048 VDC	0-1889 ppmv	$C_{\text{ppmv}} = 922 \frac{\text{ppmv}}{\text{volt}} \cdot E$

### 3.3 Available Gas Compositions

To evaluate the performance of these three sensors, seven premixed gas cylinders containing various concentrations of CO<sub>2</sub> gas were purchased from Airgas Inc, Opelika, AL. The CO<sub>2</sub> concentrations ranged from 0 to 1889 ppmv and the remaining balance

consisted of N<sub>2</sub>. The certificates of analysis provided by the supplier are shown in Appendix I. Table 5 summarizes the as-received gas compositions utilized in this study.

**Table 5:** Composition of premixed gas cylinders used in this study: The CO<sub>2</sub> concentrations were balanced with N<sub>2</sub> gas.

<b>Target Concentration (ppmv CO<sub>2</sub>)</b>	<b>Actual Concentration (ppmv CO<sub>2</sub>)*</b>	<b>Standard</b>
0	<0.5 ppmv	Research
400	400.6 ± 2%	Certified
600	591.1 ± 2%	Certified
800	797.1 ± 2%	Certified
1000	993.7 ± 2%	Certified
1500	1501 ± 2%	Certified
2000	1889 ± 2%	Certified

\* Certified by Airgas, Inc.

### 3.4 Sensor Experiments

Two sets of experiments were conducted thereby allowing both sampling methods to be evaluated. In the first set of experiments, the premixed gases were passed through the inlet and outlet ports on each sensor. In the second set of experiments, the sensors were placed in a sealed chamber filled with a known concentration of gas which diffused into the sensor.

The goal of both experiments was to determine the sensor response when exposed to a step change in concentration. The experimental procedures described below were designed to create a near instantaneous change in CO<sub>2</sub> concentration. This methodology was done to eliminate complications which arise when a sensor “chases” a time variant gas concentration. The desired concentration profile and expected sensor response are shown schematically in Figure 12.



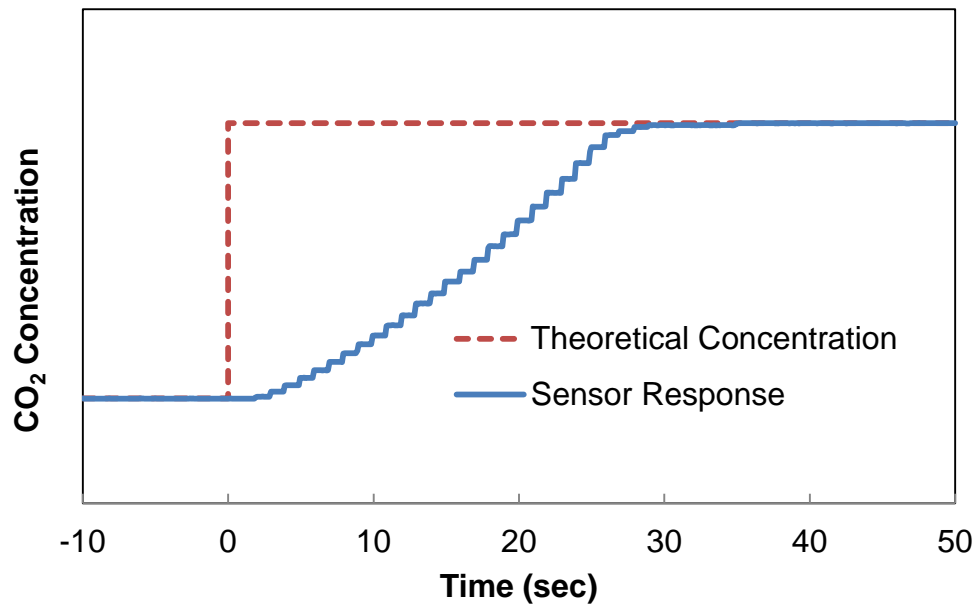


**Figure 12:** The desired CO<sub>2</sub> concentration profile (dashed line) compared to the expected sensor response (solid line)

### 3.4.1 Flowing Gas Experiments

In the first of the two test methods, premixed gasses were flowed directly into or over the sensors. The Madur madIR-D01 CO<sub>2</sub> and the Figaro K30 sensors each have ports which allow flow through the devices. The E2V IR11EJ sensor, however, does not include inlet / outlet ports. Therefore, a gassing hood provided by E2V in the evaluation kit was used to flow gas over the sensor (Figure 13).

Figure 13 shows a schematic of the overall testing apparatus used to perform the flowing gas tests. The test gas was supplied from gas cylinder connected to a nitrogen regulator set to 20 psig. The gas then flowed through a needle valve which was adjusted to control the volumetric flow rate and drop the pressure to near that of the surrounding atmosphere. A rotameter was placed downstream of this valve to monitor the flow rate.

The gas then passed through the sensor or gassing hood before being vented. Ball valves were placed up and down stream of the sensor to provide isolation capability. Since the readings of an NDIR sensor may be affected by absolute pressure, a pressure transducer was included to ensure that the system did not become pressurized.

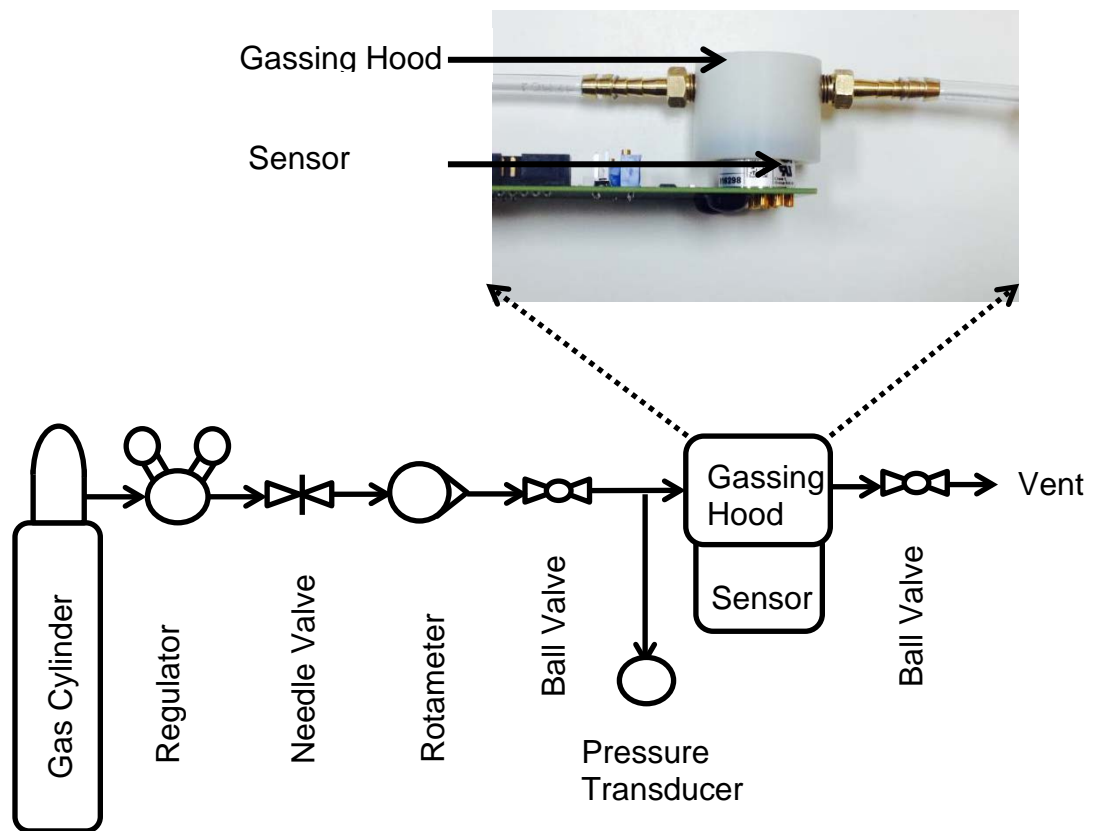


**Figure 13:** Block diagram of flowing gas apparatus with inlay showing the gassing hood on the E2V IR11EJ.

The flow rates used to test each sensor are summarized in Table 6. The Madur madIR-D01 CO<sub>2</sub> and Figaro K30 sensors were supplied gas at the flow rate specified by

the manufacturer. A flow rate was not specified by E2V for use with the gassing hood. To determine an acceptable rate for this sensor, 1889 ppmv CO<sub>2</sub> gas was flowed through the hood at various rates ranging from 0.5 L/min to 3.0 L/min in increments of 0.5 L/min. The response times decreased with increasing flow rate of the sample gas (Figure 14). Once the flow rate exceeded 3.0 L/min, the pressure in the system started to climb above ambient and the indicated CO<sub>2</sub> concentration began to increase. Therefore, the highest flow rate that did not generate a detectable increase in pressure was adopted as the flow rate for testing the E2V IR11EJ. Since the volume of the gassing hood was 7 ml, this flow rate caused the gas in the hood to be completely exchanged seven times per second.

**Table 6:** Summary of flow rates used for the flowing gas experiments

<b>Sensor:</b>	<b>Flow Rate:</b>	<b>Rate Determination:</b>
Madur madIR-D01 CO <sub>2</sub>	1.5 L/min	Provided by manufacturer.
Figaro K30	0.5 L/min	Provided by manufacturer.
E2V IR11-EJ	3.0 L/min	Experimentally determined.

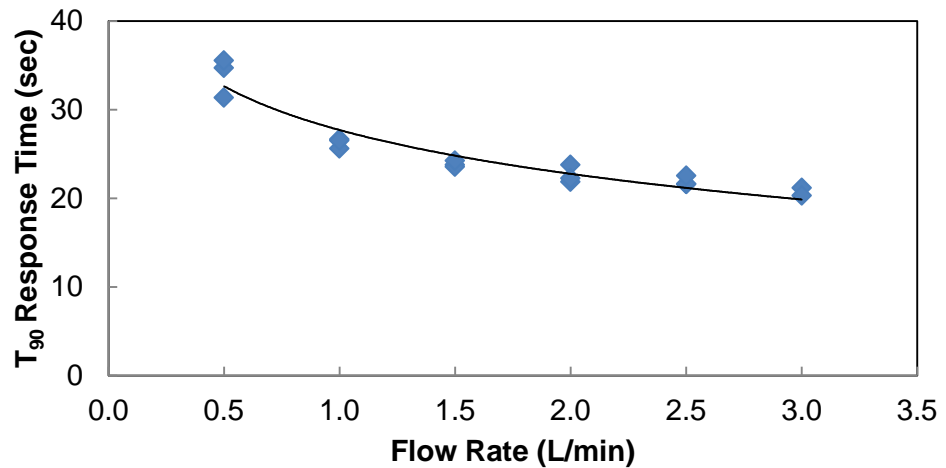


**Figure 14:** Response time of hooded E2V IR11EJ to 1899 ppmv CO<sub>2</sub> as a function of volumetric flow rate

To perform a flowing gas experiment, gas containing 400 ppmv CO<sub>2</sub> was flowed through the system to provide a known stable, initial CO<sub>2</sub> concentration for each test. Once the measured concentration stabilized, the sensor was isolated by closing the upstream and downstream ball valves. Then, the system was connected to another cylinder containing a known CO<sub>2</sub> concentration (ranging from 0 to 1889 ppmv CO<sub>2</sub>). Next, gas lines upstream of the first isolation valve were purged. This was done to prevent erroneous response times which would have occurred if the new concentration was delayed in reaching the sensors while the original concentration was forced out of the tubing. The data acquisition system was then initiated and ten seconds of concentration data were recorded to establish the initial concentration before the isolation valves were opened – thus simulating a step change in concentration. This process was followed for each CO<sub>2</sub> concentration, alternating between the highest and lowest concentrations yet to

be tested. Once all the available gas concentrations were tested, the procedure was repeated at least two more times thereby providing a minimum of three independent tests at each concentration.

### 3.4.2 Elevated Temperature Tests

To evaluate the effects of temperature on the accuracy of the sensor readings, the flowing gas experiments were modified slightly to allow the gas temperature to be controlled. A system installed immediately downstream of the first ball valve after the rotameter allowed the elevated temperatures to be generated; Figure 15 shows a schematic of this system. This configuration consisted of a water bath and heater element controlled by adjusting the power supplied by a variable transformer (variac). The gas was heated as it passed through a radiator submerged in the bath. The heated gas then flowed through additional tubing to the sensor or gassing hood inlet. The tubing downstream of the radiator was wrapped in heat tape connected to a second transformer to counteract the significant thermal losses which occurred when gas was piped through unheated tubing. A thermistor IC was placed immediately upstream of the CO<sub>2</sub> sensor inlet to monitor the gas temperature. By adjusting the water bath and heat tape transformer settings, the temperature could be maintained within 5 °F (3°C) of the target temperature.

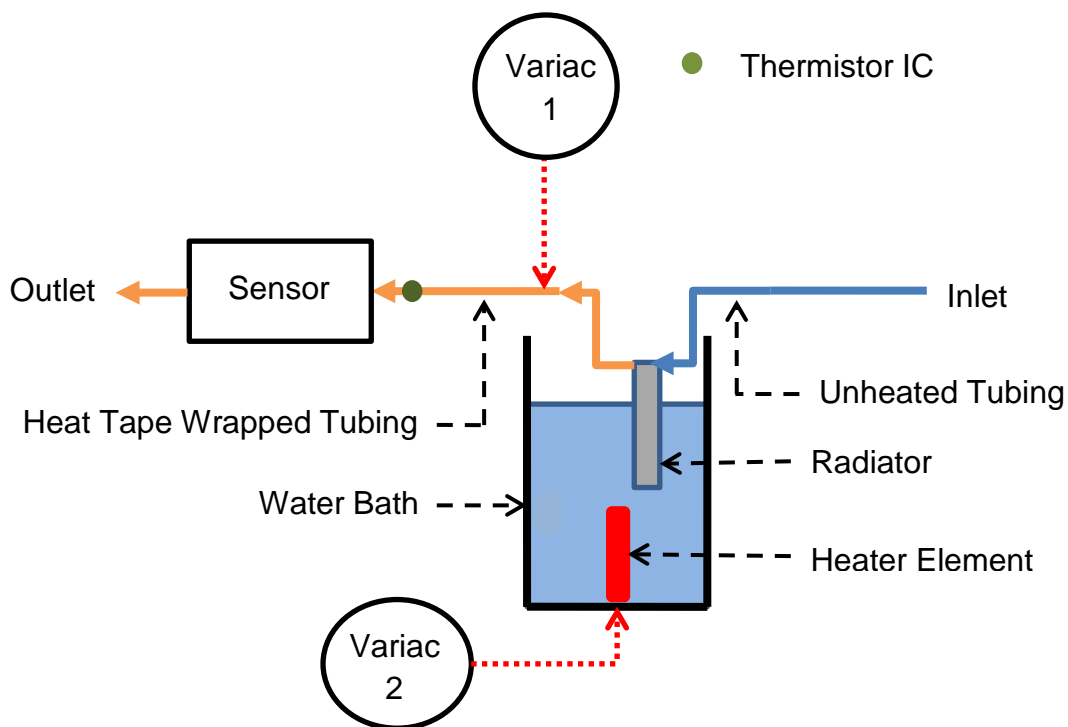


**Figure 15:** Schematic of the apparatus used to control the temperature of flowing gas

To assess the effect of temperature on sensor accuracy, test gas at each available concentration was passed through the sensor/gassing hood and the steady state values were recorded. The process was repeated with the inlet temperature set at room temperature  $\sim 72^{\circ}\text{F}$ ,  $100^{\circ}\text{F}$  and  $120^{\circ}\text{F}$  ( $22^{\circ}\text{C}$ ,  $38^{\circ}\text{C}$ , and  $49^{\circ}\text{C}$ ). The steady state readings were then compared against the known concentration of the gas and the readings collected at other temperatures.

### 3.4.3 Diffusion-Based Sampling Experiments

In addition to testing the sensors by flowing gas, another set of experiments was devised to evaluate the response of the Figaro K30 and E2V IR11EJ sensors while employing diffusion-based sampling. The Madur madIR-D01  $\text{CO}_2$  sensor was excluded

from these tests because it does not support diffusion-based sampling. Figure 16 shows a schematic of the apparatus used to conduct these tests. This apparatus includes a ten inch inner diameter acrylic tube bonded to a PVC plate on one end and capped with a removable test plug on the other.

Both sensors were placed in this chamber; an expandable latex bladder was filled with test gas thereby displacing a portion of the air previously occupying the chamber. This air was allowed to escape through an open vent port to prevent an increase in system pressure, and to protect the sensors from contact with the bladder as it expanded, a metal screen was mounted at the bottom of the chamber. To simulate a change step concentration change, the bladder was mechanically ruptured and the vent port was sealed. The test in the bladder gas mixed nearly instantaneously with the remaining gas in the chamber simulating a step change in concentration. Two fans were mounted in the top of the chamber to ensure prompt mixing. This arrangement causes complete mixing in well under one second as shown in a previous study utilizing an identical chamber [41].

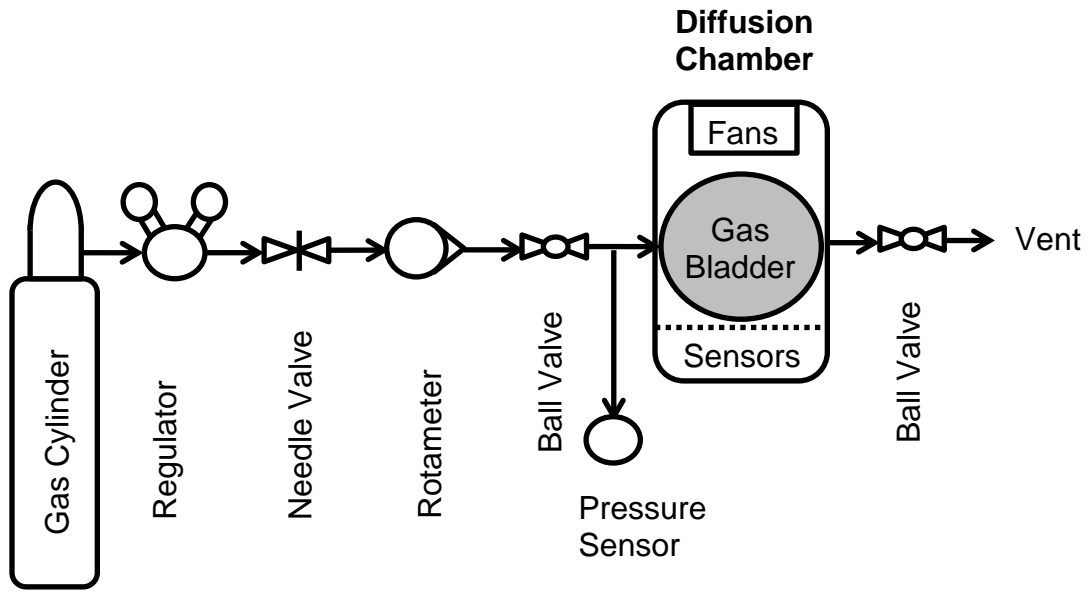


**Figure 16:** Block diagram of diffusion testing apparatus used with Figaro K30 and E2V IR11EJ sensors.

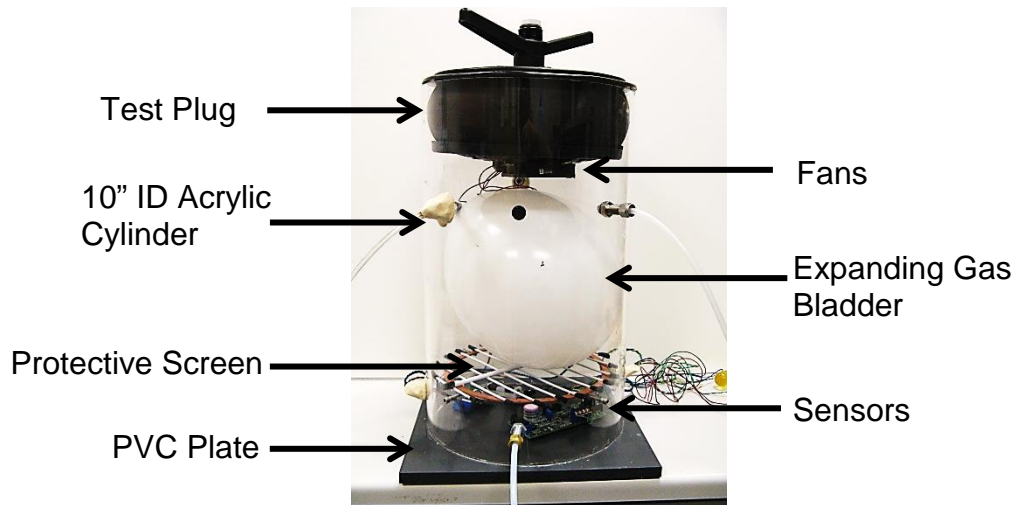


**Figure 17:** Chamber used to test diffusion-based sampling of Figaro K30 and E2V IR11EJ sensors



Before conducting a diffusion test, the system was purged. Initially, the chamber was purged with shop air. After purging, the system would reach a concentration of approximately 500 ppmv CO<sub>2</sub>. The exact concentration varied slightly based on the environmental conditions and the number of people present in the room (exhaling CO<sub>2</sub>). Next, the gas lines were connected to one of the cylinders of testing gas, and the lines upstream of the diffusion chamber ball valve were purged with the testing gas.

Once the system was purged, the bladder was then filled with the lowest concentration testing gas available with a concentration higher than the target concentration. By adjusting the fill time and volumetric flow rate, the amount of gas introduced to the bladder was varied. Regulating the concentration and amount of gas in the bladder allowed the final concentration in the chamber to be adjusted from 525 ppmv to 1000 ppmv. Because the test gases were diluted in this chamber, it was possible to blend lower concentrations than were available for the flowing gas tests; however, the maximum concentration was limited to 1000 ppmv using the available gasses.

Equation 2 shows the formula used to predict the final CO<sub>2</sub> concentration in the chamber. The first term accounts for the CO<sub>2</sub> present in the testing gas and its dilution into a larger volume. The second term accounts for CO<sub>2</sub> which was initially present in the environment.

$$C_{Final} = \frac{V_{Test\ Gas}}{V_{Chamber}} \cdot C_{Test\ Gas} + \frac{V_{Chamber} - V_{Test\ Gas}}{V_{Chamber}} \cdot C_{Initial\ Chamber} \quad \text{Eq. 2}$$

Once the bladder was filled, the data acquisition system was initialized, and ten seconds of concentration data were recorded and averaged to establish a steady initial

concentration. Next, the bladder was mechanically ruptured, simulating a step change to the concentration in the chamber. Data were collected for five minutes to ensure that the sensor was given time to reach steady state. The resulting data were then analyzed using Matlab to determine the response characteristics of each sensor.

#### 3.4.4 Micropump Experiments

The flowing gas test used undiluted gases obtained from premixed gas cylinders. As a result, the range of concentrations available for the flowing gas tests was higher than the diffusion tests. Therefore, a system was devised to generate lower concentrations of flowing gasses (Figure 18). The premixed gasses were diluted in the same chamber used in the diffusion experiments. Then micropumps were used to pump the gas through the sensor or gassing hood.

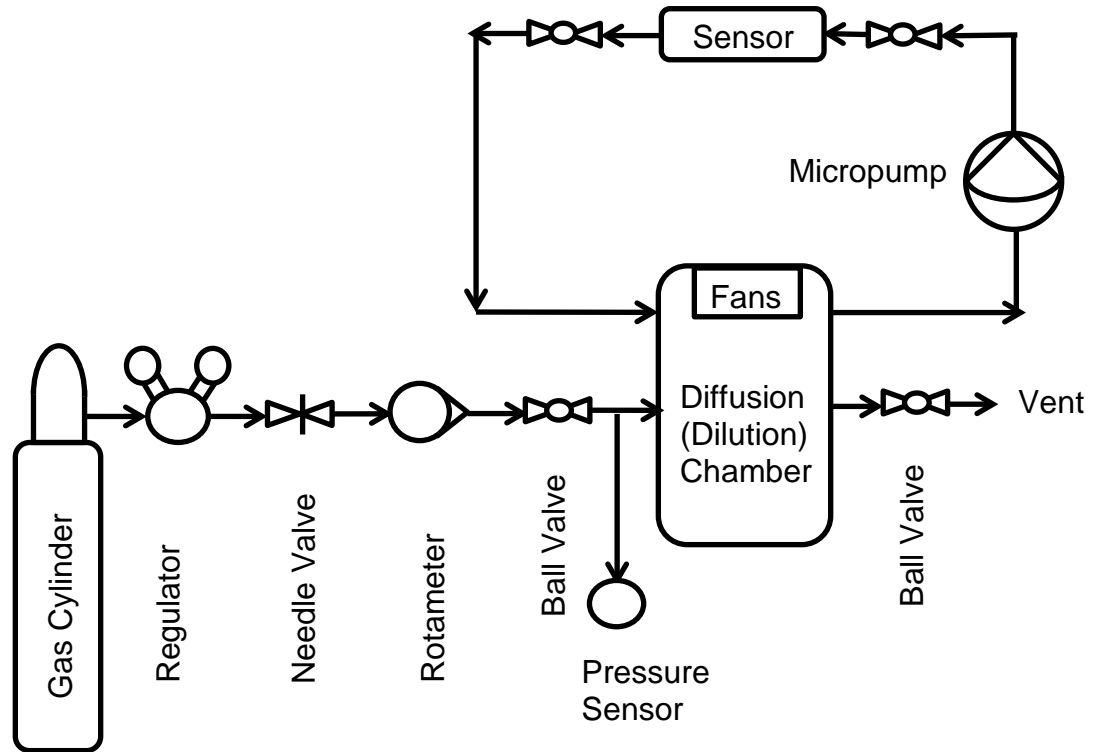


**Figure 18:** Schematic of the apparatus used to create diluted gas concentrations. A micropump is used to pump the diluted gas into the sensor.

Micropumps were used to pump gasses through the sensors at the same volumetric flow rates used in the original set of experiments. This operation required two different micropumps. A Parker Fluidics H022C-11 diaphragm pump (Figure 19) with a maximum flow rate of 3.25 L/min was used to supply the gas to gassing hood connected to the E2V IR11EJ. The gas was supplied to the Figaro K30 using a Parker Fluidics E155-11-050 diaphragm pump with a maximum flow rate of 0.650 L/min. The pumps were connected to a rotameter and the supply voltages were adjusted so that the flow rates matched the flow rates employed in the original set of flowing gas tests.



**Figure 19:** Parker Fluidics H022C-11 diaphragm pump used to provide gas to the E2V IR11EJ while conducting micropump experiments with a dime shown for size comparison.

To conduct an experiment, the appropriate sensor was placed together with the micropump in a loop which allowed the gas to circulate from the chamber to the sensor and back in the chamber. Carbon dioxide was diluted in the chamber until the sensor concentration as read by the sensor was 500 ppmv (The sensor accuracy was confirmed in previous tests). The sensor was isolated using the ball valves before being disconnected from the chamber and flushed with 400 ppmv gas. At this point, the sensor was then reconnected with the isolation valves still closed to hold the 400 ppmv concentration. The data acquisition was initialized and ten seconds of concentration data were recorded to provide a steady initial concentration. After these ten seconds, the valves were opened and the diluted gas passed through the sensor. The sensor's voltage output was recorded to determine the response of this sensor to the change in concentration.

## 4. Results and Discussion

### 4.1 Steady State Results

The steady state results were evaluated using only the data from the flowing gas experiments. This limitation was chosen because the concentrations of the gases used in the flowing gas test were well known, certified concentrations and could serve as a valid standard.

#### 4.1.1 Accuracy

To evaluate the accuracy of each sensor, the sensors were allowed to reach their final steady state values and then the final ten seconds of each test were averaged to minimize the effect of signal noise and determine the final steady state concentration. This was the value that was compared to the known concentration of the gas specified on its certificate of analysis.

All three sensors responded linearly and accurately through the range of concentrations tested (Figure 20). The most accurate sensor was the Madur madIR-D01 CO<sub>2</sub> which consistently overestimated the concentration of CO<sub>2</sub> by 1.8 percent. This accuracy was closely followed by the Figaro K30 sensor which underestimated the CO<sub>2</sub> concentration by an average of 2.0 percent. The E2V IR11EJ was the least accurate: typically underestimating the concentration by 4.2 percent.

Table 7 provides a summary of the accuracy of each sensor; more detailed information including the specific error at each measured concentration is provided in Appendix III.

**Table 7:** Summary of the accuracy of each sensor from 0 to 1889 ppmv

Sensor	Tests	Span Error (%)	0 PPMV Offset Error (ppmv)
Madur madIR-D01 CO <sub>2</sub>	24	+ 1.8	+ 13.1
Figaro K30	21	- 2.0	- 1.4
E2V IR11EJ	36	- 4.2	-12.7

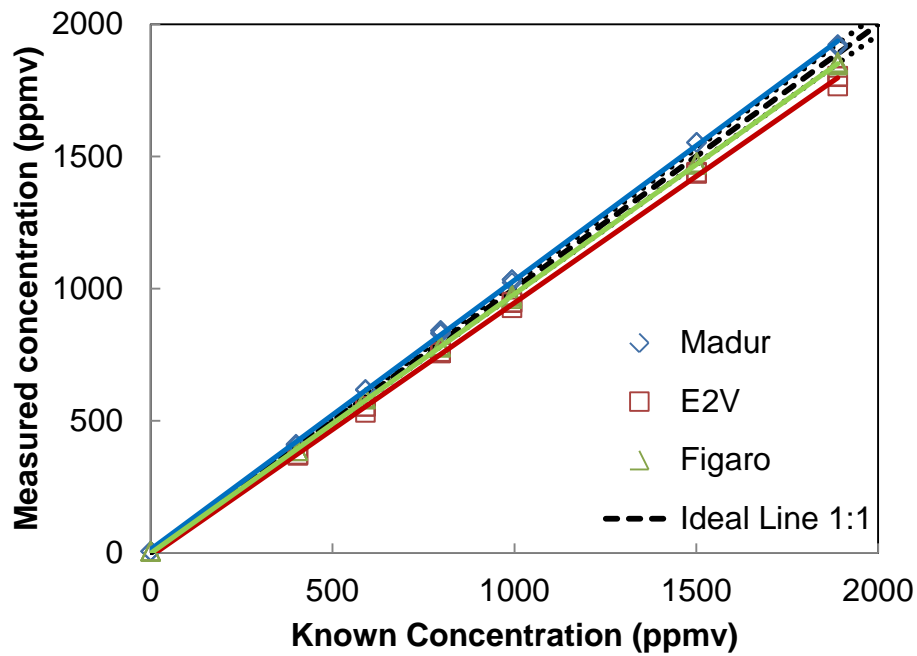


**Figure 20:** Measured reading of each sensor compared to the concentration of a set of known gasses. The dashed line indicates the ideal 1:1 ratio and the dotted bands indicate the analytical uncertainty of the known gas concentrations.

#### 4.1.2 Hysteresis

To evaluate the hysteresis properties of the sensors, the premixed, certified gasses were passed through the sensor or gassing hood. The initial concentration supplied to each sensor was 0 ppmv CO<sub>2</sub> and the concentration was serially increased after every five

minutes. Once the highest concentration available was used, the process continued by decreasing the concentration back to 0 ppmv CO<sub>2</sub>. Figure 21 shows the concentration profile used to conduct the hysteresis evaluation on each of the sensors.

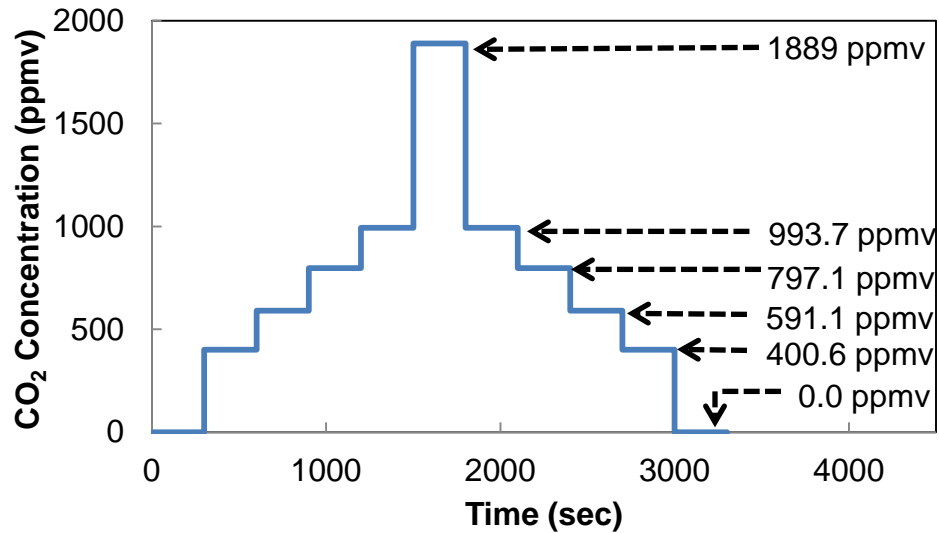


**Figure 21:** Concentration profile used to conduct a hysteresis evaluation on each sensor.

The sensor readings were given one minute to stabilize after each new concentration was introduced. Data taken during the following three minutes were then averaged to determine the steady state measurement of the sensor at each concentration. Then, after an additional minute, the next concentration was introduced into the sensor. These steady state values were plotted against the certified concentration of the gas. Figure 22 shows the steady state measurements the Madur madIR-D01 CO<sub>2</sub> taken during the hysteresis characterization. The results are typical of all the sensors evaluated and showed no detectable hysteresis.

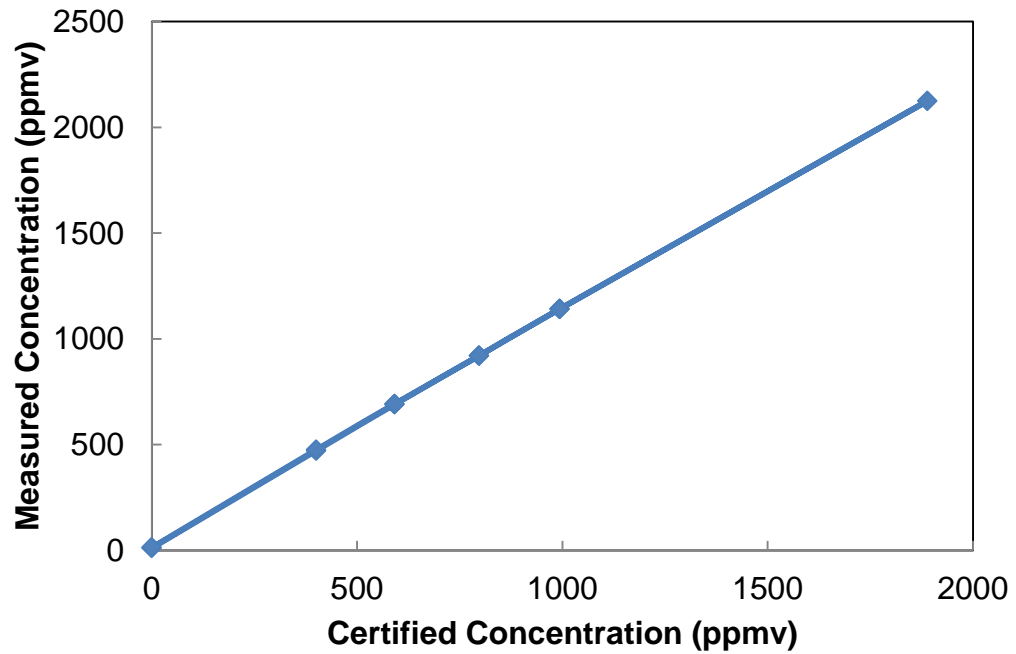


**Figure 22:** Measured CO<sub>2</sub> concentration of Madur madIR-D01 CO<sub>2</sub> during hysteresis test. The results are typical of all sensors tested showing no hysteresis loop.

#### 4.1.4 Temperature Sensitivity

The temperature of the gas can significantly affect the accuracy of a NDIR sensor if thermal effects are not considered in the algorithm used to convert infrared intensity into a concentration in ppmv. The thermal effects are dominated primarily by the thermal expansion of the gas. Expansion of the gas due to variations in temperature and pressure can easily be compensated for using the ideal-gas law. Equation 3 will convert a measured molecular concentration ( $\frac{mols}{m^3}$ ) of an ideal gas to an equivalent concentration at the temperature and pressure for which the sensor is calibrated. Both the temperature and pressures values used in this calculation must be in absolute units.



$$C_{Equivalent} = \frac{T \cdot P_{Cal}}{T_{Cal} \cdot P} \cdot C_{Measured} \quad \text{Eq. 3}$$

It is important to note that the true concentration in ppmv does not vary with temperature or volume. However, the temperature and pressure compensation must still be applied. NDIR sensors do not physically measure the gas concentration directly in ppmv. Instead, they measure the absorbance of infrared radiation which is a function of molecular concentration according to Beer-Lambert's law. Then built-in algorithms convert the molecular concentration to a concentration into a ppmv. These algorithms typically assume that the pressure remains at one atmosphere. Unfortunately, some sensors do not monitor the actual temperature of the gas and thus cannot correct for temperature changes.

Additional thermal effects influencing the sensor measurement are due to temperature induced changes in the sensor itself. Temperature can affect the infrared filter characteristics, pyroelectric detector outputs and the mechanical/optical alignment. However, if the operating range of the sensor is restricted to -40 to 75 °C (-40 to 167 °F) and the pressure is held constant, the combined effect of the gas expansion and thermally induced changes in the sensor is linear [30].

To measure the effect of gas temperature on the accuracy of the sensor readings, a set of experiments was conducted in which the temperature of the flowing gas was held at room temperature and then elevated to 100 °F (38°C) and 120 °F (49°C) while one atmosphere of pressure was maintained.

All three sensors which were evaluated in this study provide on-board temperature compensation. However, unlike the other sensors evaluated, the temperature

sensor on the Madur madIR-D01 CO<sub>2</sub> is not located in the gas path; it is instead located on the printed circuit board. As a result, the temperature correction for this sensor will only work properly if the board is held at the same temperature as the gas passing through the sensor.

Figure 23 shows the steady state measurements recorded by at the madIR-D01 CO<sub>2</sub> for each of the known concentrations at three different temperatures. The lines representing each temperature do not overlay indicating that the temperature compensation was not working properly. This result was expected because the experimental procedure employed heated only the gas and not the sensor board. When the ideal gas law correction was applied to the sensor readings, the response of the sensor became effectively temperature independent as expected (Figure 24).

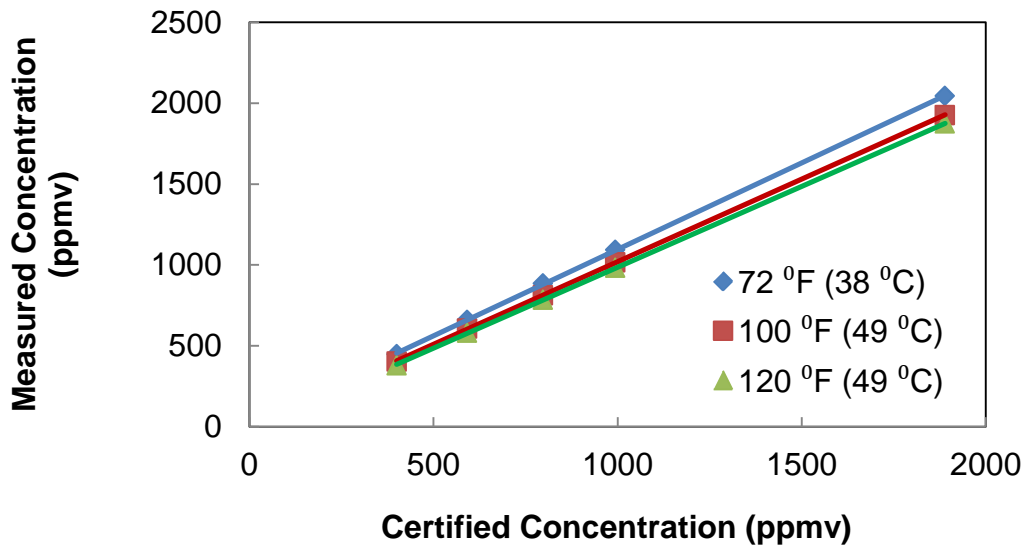


**Figure 23:** Chart showing steady state measurements recorded by the Madur madIR-D01 CO<sub>2</sub> at various temperatures to known gas concentrations before applying ideal gas law calibration.

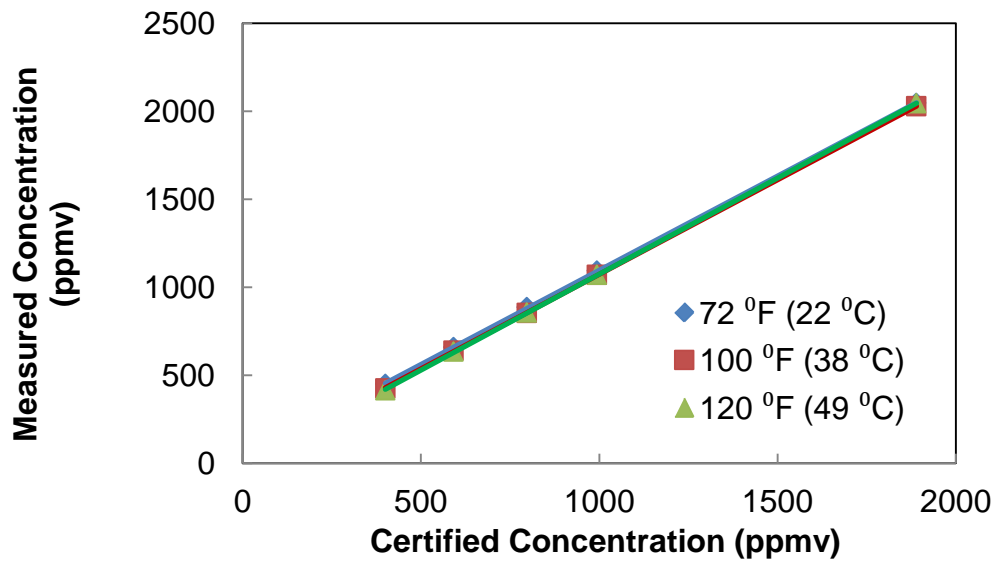


**Figure 24:** Chart showing the steady state measurements recorded by the Madur madIR-D01 at various temperatures to known gas concentrations after applying the ideal gas law calibration.

The E2V IR11EJ and Figaro K30 devices include built-in temperature compensation, and the temperature sensor in each device is located in the gas path. The compensation algorithm worked properly under the conditions examined causing the lines representing the various temperatures to overlay (Figure 25 and Figure 26).

The E2V IR11EJ readings show a slight offset between the room temperature and the other two temperatures tested. However, this difference is believed to be due to sensor drift and not temperature effects. The tests were conducted on two different days, and temperature effects would cause the sensor readings at the various temperatures to be nonparallel if there were thermally induced errors.

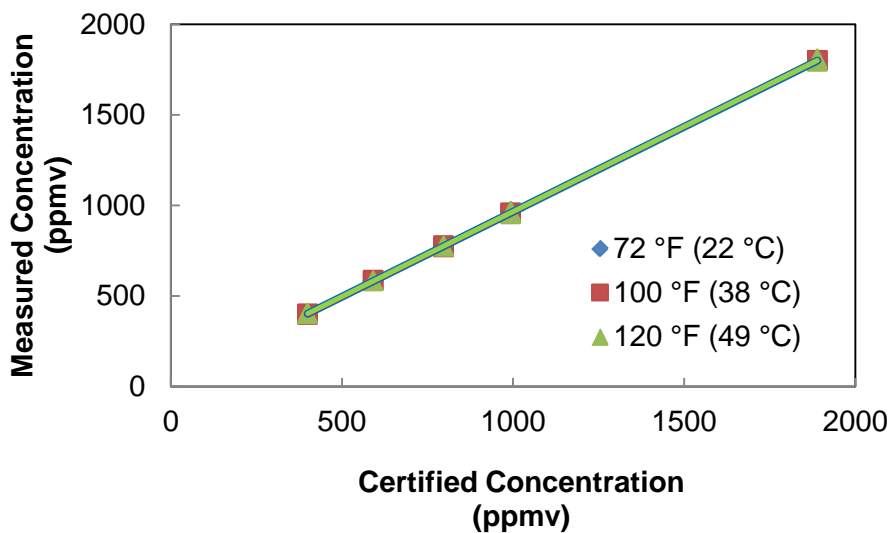


**Figure 25:** Steady state measurements recorded by the Figaro K30 at various temperatures to known gas concentrations

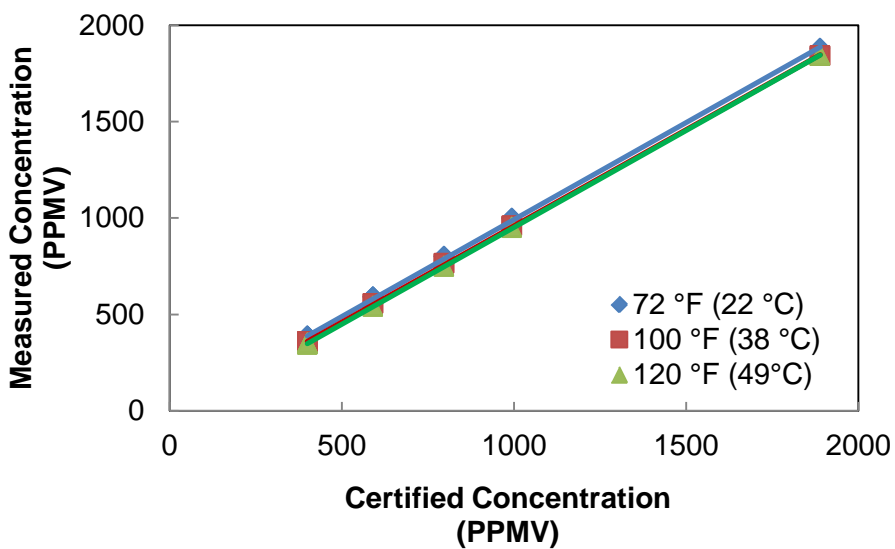


**Figure 26:** Steady state measurements recorded by the E2V IR11EJ at various temperatures to known gas concentrations

### 4.1.3 Noise

The voltage output from each sensor updated once per second, and remained constant until the next update. Consequently, the signals from these sensors form stepwise functions. The minimum step size is determined by whichever is smaller: either the resolution of the sensor or its digital to analogue converter (DAC) which provides the voltage output. This step size is not always constant across the range of the sensor. The resolution of the madIR-D01 CO<sub>2</sub> is 1 ppmv when the CO<sub>2</sub> concentration is less than one third of its operating range (<833 ppmv) and 10 ppmv when the measured concentration is greater than one third of its range. The minimum step size of the Figaro K30 is 5 ppmv across the sensors entire range of the sensor; this sensor is limited by the resolution of the analogue output. The resolution of the E2V IR11EJ evaluation board pair is not specified; however, observations have shown steps as small as 1 ppmv.

There is noise introduced in sensor readings both before and after readings are converted to a voltage signal. If the noise which is introduced into the readings before the DAC is greater than the minimum step size, there will be a series of steps that fluctuate about the actual CO<sub>2</sub> concentration. The noise introduced after the DAC results in steps which are not flat, constant values. This post-DAC noise can become significant enough to prevent identification of individual steps.

Figure 27 illustrates the stepwise function of the analogue outputs as well as pre-DAC and post-DAC noise. In the first ten seconds, pre-DAC noise is visible; it causes a series of steps which fluctuate about 441 ppmv. In the middle of the test, the stepwise sensor response is visible in the transition from the initial and final concentration. The post-DAC noise is visible throughout the entire test.

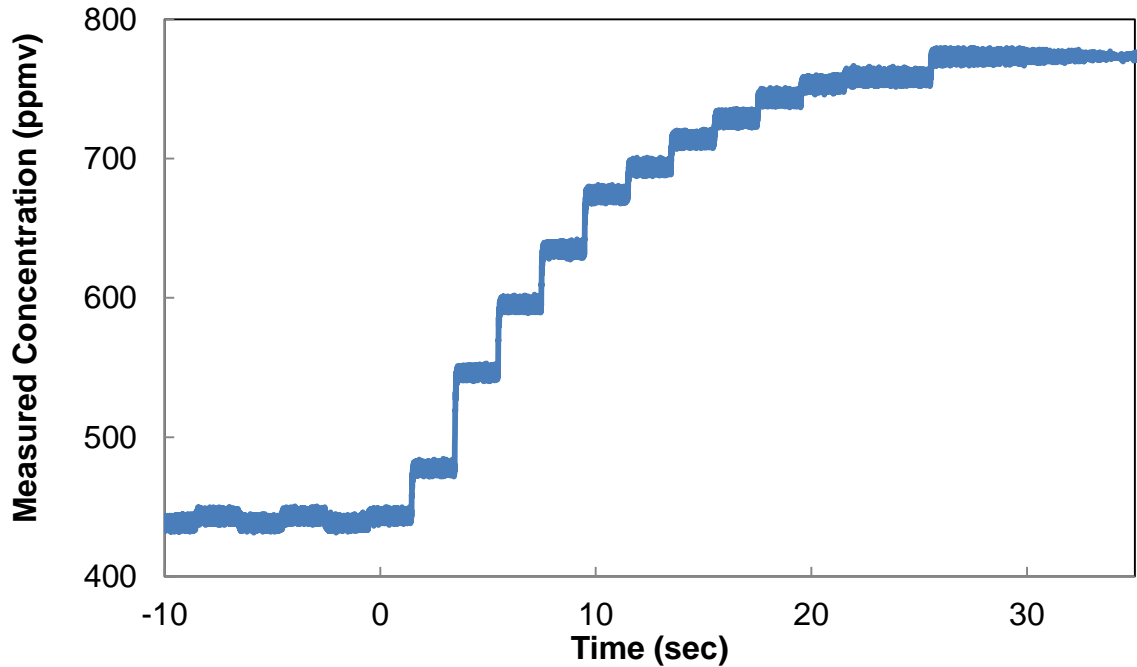


**Figure 27:** Response of the Figaro K30 sensor a flowing gas experiment illustrating the both stepwise response and noise present in the signal. The concentration was changed from 400 ppmv to a 797.1 ppmv near instantaneously when the time was equal to zero.

The sensor noise was quantified by determining the root-mean-square (RMS) noise present in the last ten seconds of the flowing gas tests. During the final ten seconds, a known concentration of gas was flowing and the sensor output had reached equilibrium. Equation 4 provides the formula used to calculate the RMS noise. In this equation,  $N$  represents the number of data points. A given reading is represented by  $x_i$ , and the average reading is represented by  $\bar{x}$ .

$$x_{RMS} = \sqrt{\frac{1}{N} \cdot \sum_{i=1}^{i=N} (x_i - \bar{x})^2} \quad \text{Eq. 4}$$

Table 8 provides a summary of the noise detected in the output signal of each sensor. The noise levels ranged from 1.0 ppmv with the Madur madIR-D01 CO<sub>2</sub> to 4.0 ppmv with the E2V IR11EJ. The results correspond to the range of the analogue voltage outputs. With a larger output range, the same variation in voltage levels corresponds to a smaller change in concentration. Therefore, the signal from the Madur madIR-D01 CO<sub>2</sub> with an analogue voltage output which ranges from 0 to 10 VDC has the least noise while the signal from the E2V IR11EJ with a voltage output ranging from 0 to 2.048 VDC is the noisiest.

**Table 8:** Summary of RMS noise evaluation of each sensor without running average

Sensor	Number of Tests	RMS Noise (mV)	STDEV (mV)	RMS Noise (ppmv)	STDEV (ppmv)
MADUR madIR-D01 CO <sub>2</sub>	18	4	5	1.0	1.1
E2V IR11EJ	15	4	1	4.0	1.0
Figaro K30	26	7	4	3.2	1.8

If a running average of one second is applied, the amount of noise can be reduced considerably with minimal loss of information. The data acquisition system has a sampling rate (60 Hz) which exceeds the update rate of the sensor (1 Hz). Consequently, it is possible to perform a running average over a one second interval. Since this is less than or equal to the refresh rate of the sensor, all the features of the data are still present, but it reduces a percentage of the noise. Table 9 shows the effect off the running average at reducing the RMS noise present in the signal output. The greatest effect was in the



noise present in the Figaro K30 which was reduced to thirteen percent of the original noise: a decrease from 3.2 ppmv to 0.4 ppmv.

**Table 9:** Summary of the noise evaluation of each sensor with a one second running average applied.

<b>Sensor</b>	<b>Number of Tests</b>	<b>RMS Noise (ppmv)</b>	<b>STDEV (ppmv)</b>
MADUR madIR-D01 CO <sub>2</sub>	18	0.6	1.3
E2V IR11EJ	15	3.1	0.9
Figaro K30	26	0.4	0.7

#### 4.2 Transient Results

To characterize the transient response of the sensors, two parameters were evaluated: time to detection and response time. This transient response was evaluated under two sets of conditions. In the first set of experiments, the gas was flowed through inlet and outlet ports integrated into the sensor. In the second set of experiments, the gas was allowed to diffuse into the sensor from the surrounding environment.

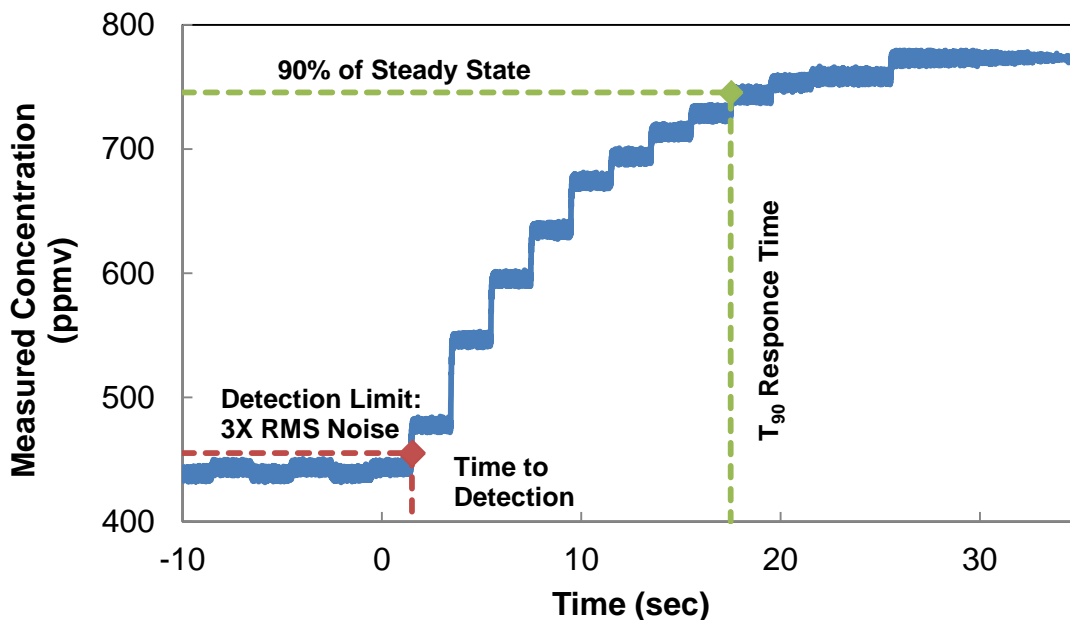


**Figure 28:** Response of the Figaro K30 sensor to a flowing gas experiment illustrating the two transient parameters: time to detection and response time. The concentration was changed from 400 ppmv to a 797.1 ppmv near instantaneously when the time was equal to zero.

#### 4.2.1 Time to Detection

The limit of detection is the smallest change in concentration which can be reliably distinguished from the background noise of the signal. Three times RMS noise was adopted as the limit of detection in this study. This value is commonly used as the limit of detection in analytical chemistry [42]. Table 10 summarizes the limits of detection for each of the sensors based on the RMS noise described in section 4.1.3.

**Table 10:** Limits of detection for the three sensors

<b>Sensor</b>	<b>RMS Noise (ppmv)</b>	<b>Limit of Detection (ppmv)</b>
MADUR madIR-D01 CO <sub>2</sub>	1.0	3.0
E2V IR11EJ	4.0	12.0
Figaro K30	3.2	9.7

The time to detection is the amount of time which is required to exceed this threshold after the onset of an event. The time of detection was found to be independent of the final concentration and also was consistent between the flowing and diffusion based sampling methods. Table 11 summarizes the time required to exceed the three times RMS threshold for each sensor. For all three sensors, the limits of detection were in the two to three second range.

**Table 11:** Time to detection for each sensor

<b>Sensor</b>	<b>Flowing Gas</b>			<b>Diffusion</b>		
	<b>Tests</b>	<b>Detection Time (sec)</b>	<b>STDEV (sec)</b>	<b>Tests</b>	<b>Detection Time (sec)</b>	<b>STDEV (sec)</b>
MADUR madIR-D01 CO <sub>2</sub>	18	2.2	0.6	N/A	N/A	N/A
E2V IR11EJ	15	3.1	0.9	10	2.5	0.3
Figaro K30	27	1.7	0.6	10	3.1	2.8

#### 4.2.2 Response Time

The response times of the sensors were evaluated by measuring the times to reach ninety percent of the steady state values achieved during the tests. A one-second, double-sided running average was applied to smooth out the noise and allow the ninety percent

value to be easily identified. Each sensors response times were characterized by using both the flowing gas and diffusion sampling methods.

#### *4.2.2.1 Flowing Gas Experiments*

Using the flowing gas technique, the response time of the Madur madIR-D01 CO<sub>2</sub> was found to be 25 seconds and independent of concentration. The concavity of the response profile decreases with increasing concentration; however, by the ninety percent mark, the response profiles converged. This is likely the effect of the sensors internal averaging routine [Appendix IV]. Figure 29 shows the response of the Madur madIR-D01 CO<sub>2</sub> to the flowing gas tests.

The concentrations were normalized using equation 5 for easier comparison. In this equation,  $C_N$  is the normalized concentration, and  $C$  is the measured concentration. The initial and final concentrations are represented by  $C_0$  and  $C_f$  respectively.

$$C_N = \frac{C - C_f}{C_f - C_0} \quad \text{Eq. 5}$$

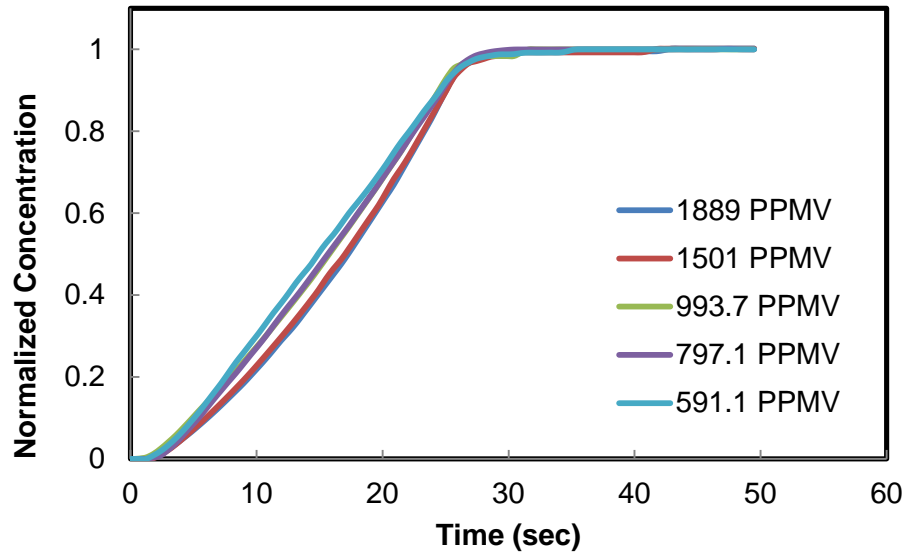


**Figure 29:** Normalized response of the Madur madIR-D01 CO<sub>2</sub> sensor to the flowing gas experiments. The concentration was changed from 400 ppmv to a variety of concentrations near instantaneously when the time was equal to zero.

The response times observed for the E2V IR11EJ sensor using the gassing hood were also found to be independent of concentration. The sensor consistently responded in 28 seconds to the flowing gas experiments. Figure 30 shows the normalized response of the sensor from 400 ppmv to a range of final concentrations. The spike which is seen at the start of the test is due to the momentary increase in pressure due to the on-rush of gas when the valves were first opened.

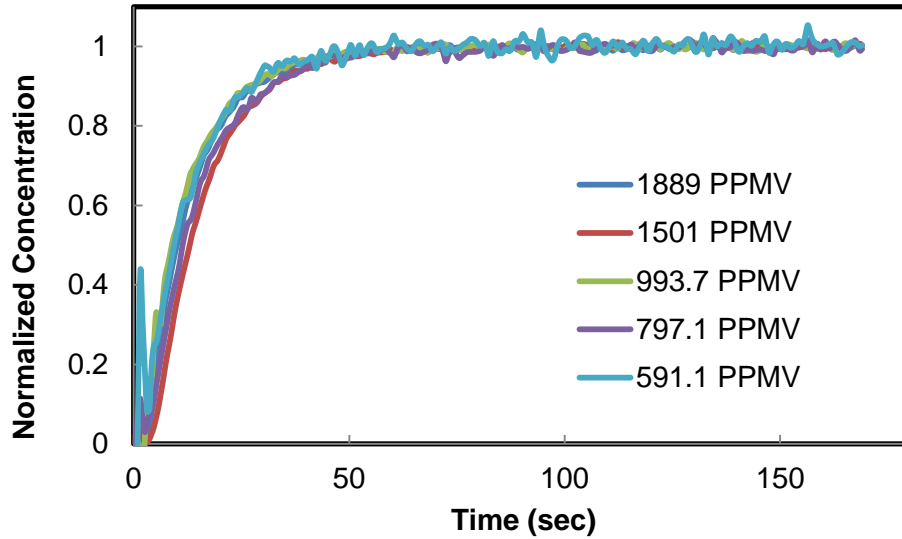


**Figure 30:** Normalized Response of the E2V IR11EJ sensor to the flowing gas experiments. The concentration was changed from 400 ppmv to a variety of concentrations near instantaneously when the time was equal to zero.

The response time for the Figaro K30 was found to be 20 seconds for the 797.1 ppmv and above concentrations. However, the 591.1 ppmv concentration required significantly longer time, i.e., 52 seconds, to reach ninety percent of steady state (Figure 31). The 591.1 ppmv tests were performed at the same manufacturer specified flow rates and similar conditions as the other concentrations. Therefore, the delayed response time is a result of an inherent property of the sensor or algorithm and not limited by delivery of gas into the sensor. Most likely, the sensor was using a different algorithm at low concentrations than it utilized at the higher concentrations. This difference could be programmed in order to improve the accuracy of the sensor by increasing the period over which the sensor internally averages the readings before outputting an analogue signal. Additional work is needed to fully understand this behavior with the Figaro K30 device.

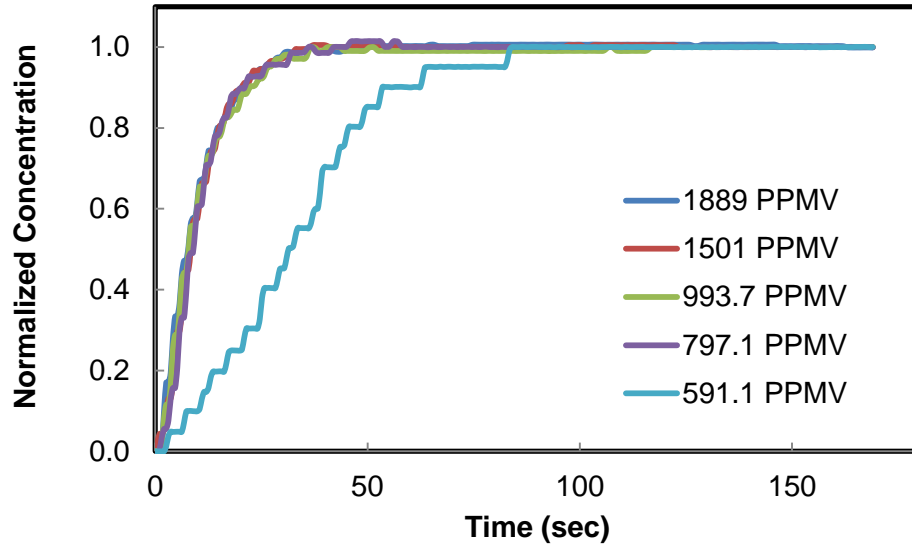


**Figure 31:** Normalized Response of the Figaro K30 sensor to the flowing gas experiments. The concentration was changed from 400 ppmv to a variety of concentrations near instantaneously when the time was equal to zero.

Table 12 summarizes the response times of each of the sensors while sampling flowing gas. As noted above, the time for the Figaro K30 to reach a steady state value of 591.1 ppmv was significantly longer than the time required to reach each of the other concentrations tested. Thus only the concentrations greater than 600 ppmv are shown in the table. The response times ranged from 20 seconds for the Figaro K30 sensor to 28 seconds for the E2V IR11EJ. These response times were consistent considering that the value output from each sensor only updated once per second.

**Table 12:** Response times obtained from the flowing gas tests

Sensor	Number of Tests	Rise Time 0-90% (sec)	STDEV (sec)
Madur madIR-D01 CO <sub>2</sub>	18	24.9	0.3
E2V IR11EJ	15	28.4	2.6
Figaro K30	21	19.8	1.6

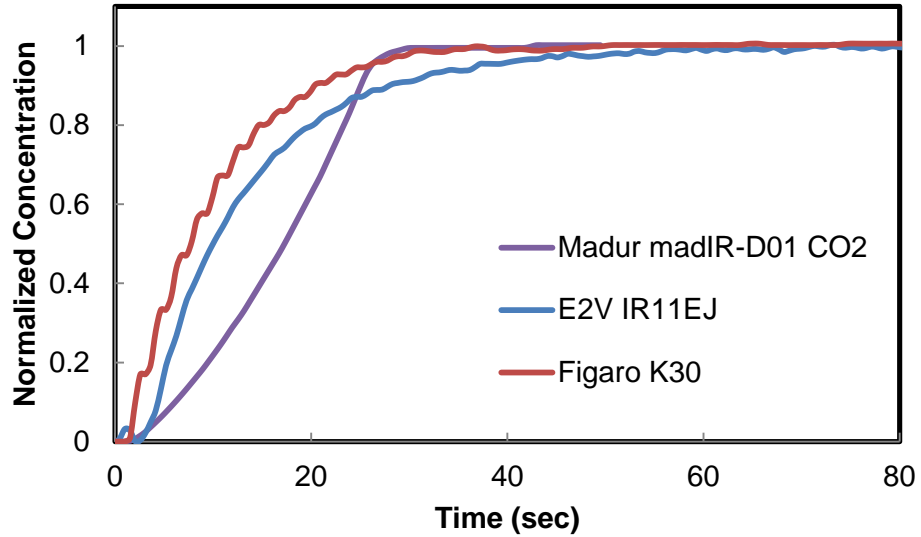


**Figure 32:** Comparison of the normalized response of three sensors to flowing gas experiment. The concentration was changed from 400 ppmv to 1889 ppmv near instantaneously when the time was equal to zero.

#### 4.2.2.2 Diffusion Experiments

The response times of the Madur madIR-D01 CO<sub>2</sub> were excluded from this round of testing because the Madur madIR-D01 CO<sub>2</sub> sensor does not support diffusion based sampling.

The response times observed during the diffusion based testing of the both E2V IR11EJ (Figure 33) and Figaro K30 (Figure 34) showed that the response times became significantly longer and more inconsistent when the difference between the initial and final concentrations was small, less than approximately 200 ppmv.



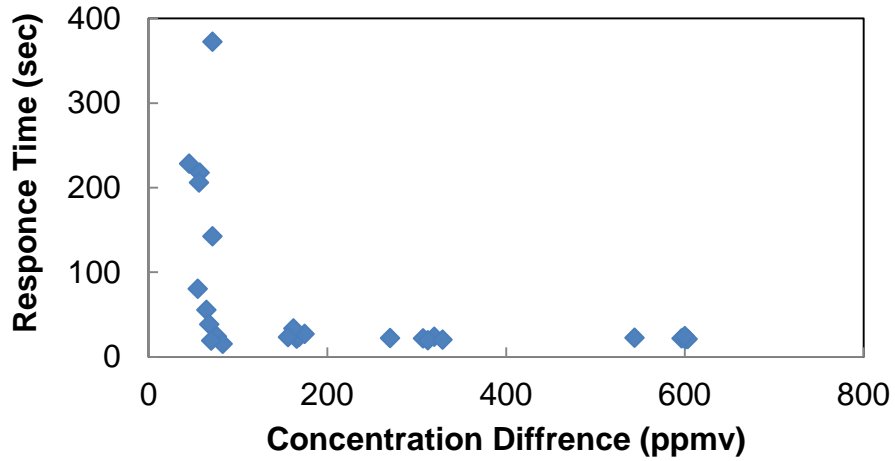


**Figure 33:** Response time of E2V IR11EJ employing diffusion based sampling as a function of concentration difference between initial and final concentrations.

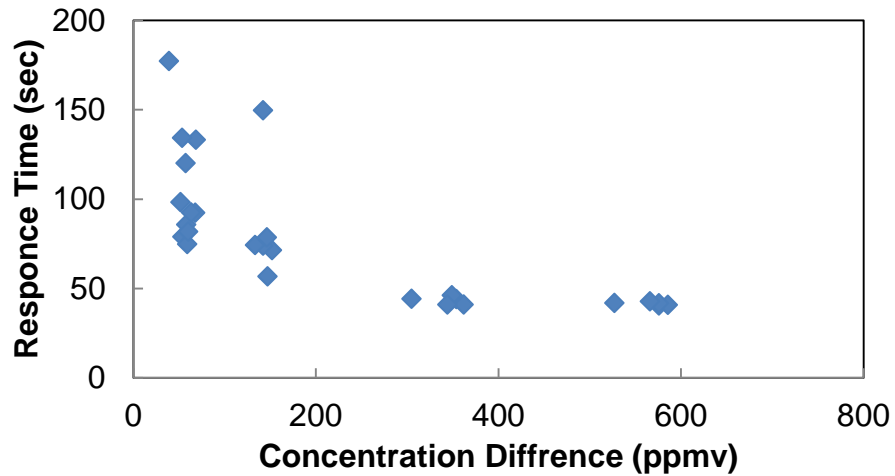


**Figure 34:** Response time of Figaro K30 employing diffusion based sampling as a function of concentration difference between initial and final concentrations.

When the difference between initial and final concentrations was greater than 200 ppmv, the responses times diminished and become consistent. It is hypothesized that these long erratic response times occur because a small concentration differential produces a weak driving force for diffusion. With higher concentration gradients, the gas

diffuses quickly into sensor, and gas sample collection is not the limiting factor driving response times. At low concentration gradients, the rate of diffusion decreases, and the response time of the sensor becomes limited by the rate of gas delivery. Other effects such as convection can become significant in determining the delivery rate and small changes in these parameters results in the long and erratic response times.

. The Figaro K30 took almost twice as long to respond when using the diffusion method instead of flowing gas sampling; the response time increased from 20 to 42 seconds. The E2V IR11EJ responded slightly faster with the diffusion testing increasing from 28 to 22 seconds.

**Table 13:** Response times of the E2V IR11EJ and Figaro K30 sensors obtained using diffusion based sampling with a difference between initial and final concentration greater than 200 ppmv.

Sensor	Number of Tests	Rise Time (sec)	STDEV(sec)
E2V IR11EJ	10	21.7	1.5
Figaro K30	10	42.4	1.9

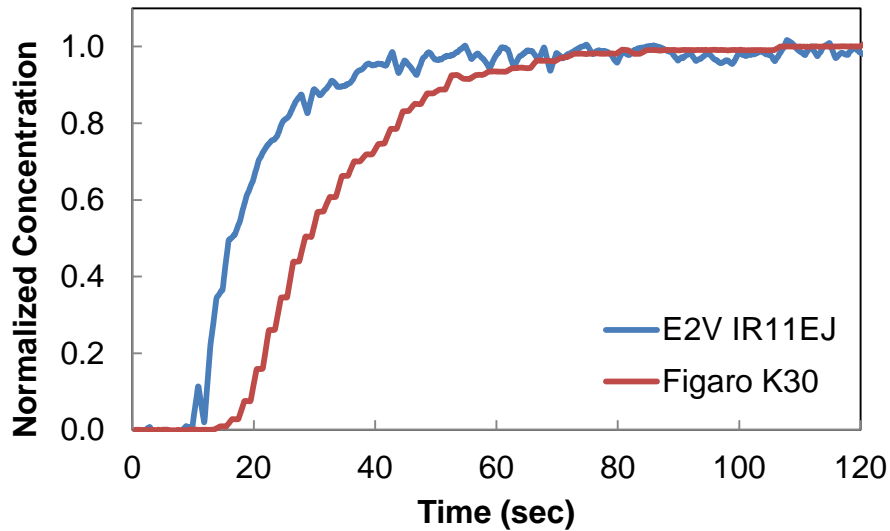


Figure 35: Normalized Response of the E2V IR11EJ and Figaro K30 sensor to the diffusion experiments. The concentration was changed from 554.71 ppmv to 1081.78 near instantaneously when the time was equal to zero.

It is hypothesized that these long erratic response times occur because a small concentration differential produces a weak driving force for diffusion. With higher concentration gradients, the gas diffuses quickly into sensor, and gas sample collection is not the limiting factor driving response times. At low concentration gradients, the rate of diffusion decreases, and the response time of the sensor becomes limited by the rate of gas delivery. Other effects such as convection can become significant in determining the delivery rate and small changes in these parameters results in the long and erratic response times.

#### 4.2.2.3 Micropump Experiments

To provide additional support for this hypothesis, it was necessary to compare the diffusion based sampling to another sampling method. If the long erratic response times were not present in a second sampling method under similar conditions, the outcome

would indicate that this phenomenon was result of the sampling method and not another inherent property of the sensors. However, the increment between the available concentrations of premixed gases was too large to create small changes in concentration using the flowing gas system. Therefore, a system (described in section 3.4.4) was created which used the same chamber employed in the diffusion tests to dilute the available gases. Then micropumps moved the diluted gasses through the sensors to get a flowing gas response time.

The long, inconsistent response times seen with low concentration differences in the diffusion experiments were not seen in the Figaro K30 micropump response times (Table 14). The sensor was slower to respond to the set of experiments with smallest concentration difference. However, the response using micropumps was several hundred seconds faster and more consistent than the response of the sensor under similar conditions while employing diffusion based sampling. This result supports the proposition that the slow, erratic response times observed in the diffusion tests result from the diffusion sampling method.

The relatively slight increase in response time of the lowest concentration difference micropump test can be attributed to the fact that the final concentration was less than 600 ppmv. A similar increase in response time was seen in the flowing gas tests at low concentrations. It is hypothesized that the sensor uses a different algorithm at lower concentrations, less than 600 ppmv.

**Table 14:** Response time of Figaro K30 to micropump experiments

<b>Concentration Difference (ppmv)</b>	<b>Number Of Tests</b>	<b>Average Initial Concentration (ppmv)</b>	<b>Average Final Concentration (ppmv)</b>	<b>0-90% Rise Time (sec)</b>	<b>0-90% STDEV (sec)</b>
122	8	394.2	515.7	49.3	5.5
217	3	405.5	623.0	17.9	0.5
1321	3	392.9	1713.7	19.7	0.2

The E2V IR11EJ consistently responded in approximately thirteen seconds when the micropumps were used, regardless of the difference between final and initial concentrations (Table 15). Conversely, the response times were long and erratic at low concentrations in the diffusion experiments. This difference indicates that the long response times seen in the diffusion tests were a function of the sampling method.

**Table 15:** Response time of E2V IR11EJ to micropump experiments

<b>Concentration Difference (ppmv)</b>	<b>Number of Tests</b>	<b>Average Initial Concentration (ppmv)</b>	<b>Average Final Concentration (ppmv)</b>	<b>0-90% Rise Time (sec)</b>	<b>0-90% STDEV (sec)</b>
97	11	403.6	501.4	14.1	2.2
1478	9	390.2	1868.1	12.7	0.6
<b>All Tests</b>	<b>20</b>	<b>N/A</b>	<b>N/A</b>	<b>13.5</b>	<b>1.8</b>

The response times observed for the E2V IR11EJ were faster during the micropump experiments, 13 seconds, than the flowing gas experiments, 28 seconds. Therefore, it is posited that in the original set of flowing gas tests, the gas flowed over the sensor without being forced into the sensor itself. When the diaphragm pumps were used, the flow was pulsatile and this encouraged movement of the gas into the sensor.

#### 4.2.2.4 Baffle Experiments

To confirm this hypothesis, the 1889 ppmv flowing gas and micropump tests were repeated with a baffle placed into the hood. This baffle was designed to force the gas to travel through the sensor rather than passing only through the gassing hood (Figure 36).

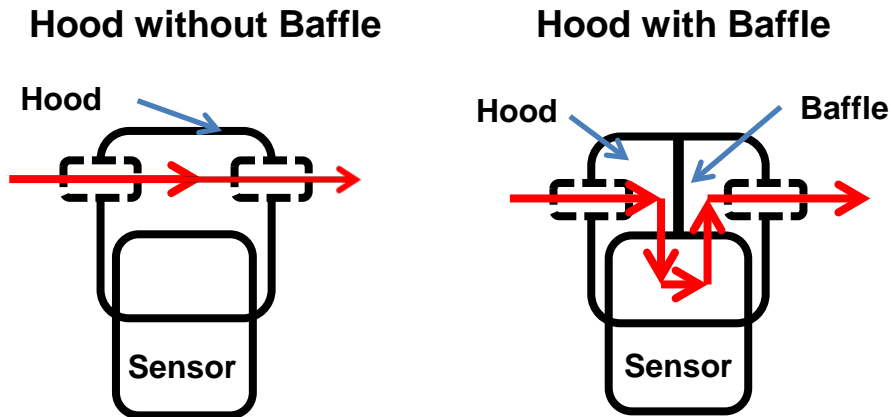


**Figure 36:** Comparison of flowing gas tests with and without baffle incorporated in the gassing hood

Table 16 summarizes the effect of the baffles on the E2V IR11EJ response time. The response time of the flowing gas experiments improved dramatically with the addition of the baffle. Once the baffle was added, there was not a significant difference between the flowing gas and micropump response times. This finding indicates that the response time of the E2V IR11EJ was limited by the method of introduction of gas into the sensor.

**Table 16:** Effect of baffles on E2V IR11EJ response times

<b>Test Series</b>	<b>Number of Tests</b>	<b>Rise Time (sec)</b>	<b>STDEV (sec)</b>
Flowing Without Baffle	15	28.4	2.6
Flowing With Baffle	5	14.6	0.5
Pumped Without Baffle	20	13.5	1.8
Pumped With Baffle	5	12.4	0.1

## 5. Conclusions

Three commercial, non-dispersive infrared CO<sub>2</sub> sensors were procured and both the steady state and transient response of the sensors were characterized. The three sensors were linear and accurate. The Madur madIR-D01 CO<sub>2</sub> and Figaro K30 reliably measured within two percent of the certified concentration when tested at CO<sub>2</sub> concentrations from ~400-1900 ppmv. Similarly, E2V IR11EJ sensor read within five percent of the certified concentration.

As a result of on-board temperature compensation, the CO<sub>2</sub> concentrations measured by the sensors were not significantly affected by temperature. However, unlike the other two sensors, the temperature sensor on the Madur madIR-D01 CO<sub>2</sub> was located on the board and only responds correctly if the board is held at the same temperature as the air flowing through the sensors.

The sensors were capable of detecting an event within two to three seconds and quickly reached steady state. When sampling with flowing gas, the response times ranged from 20 sec to 28 seconds with the Figaro K30 and E2V IR11EJ respectively. When a baffle was added to the hood, the E2V IR11EJ flowing gas response time improved reaching 12 seconds making it the fastest responding sensor.

The response times observed while employing diffusion based sampling were long and inconsistent when the concentration change was less than 200 ppmv. At



concentrations greater than 200 ppmv, the response times ranged from 22 seconds to 43 seconds with the E2V IR11EJ and Figaro K30, respectively. Consequently, it is recommended that the flowing gas sampling method be used to provide faster and more consistent response times, especially when measuring small concentration changes.

In aviation applications, space and weight are important considerations as well as accuracy, stability and response time. The Figaro K30 and E2V IR11EJ sensors show potential to monitor the bleed air system for contamination or to provide demand control ventilation allowing the mix between recirculated and fresh air to be optimized for maximum efficiency and comfort. These two sensors are small, lightweight devices which provide accurate concentration measurements. However, despite being the most accurate and fastest responding in flowing tests, the Figaro K30, unlike the E2V IR11EJ, is a single wavelength sensor. Therefore, without baseline correction, the Figaro K30 concentration measurements are likely to drift over time and require more frequent calibration. The Madur madIR-D01 CO<sub>2</sub> provides a fast, accurate response, but it is considerably larger and heavier than the other sensors tested.

## **6. Future Work**

Two important characteristics of the sensors remain to be tested: long-term stability and pressure effects. If NDIR sensors are adopted for use in the aerospace industry, the time between calibrations should be minimized to reduced maintenance costs and aircraft down-time. Accordingly, long term stability tests should be conducted with test periods exceeding six months. Additionally, sensor manufacturers claim that pressure effects can be easily accounted for using a correction based on the ideal gas law. Given the pressure fluctuations onboard an aircraft, the sensors should be tested to ensure that they perform as intended under reduced pressure conditions.

The three non-dispersive infrared sensors evaluated performed well in laboratory conditions. However, it is important to evaluate the effectiveness of the sensors in more real-world conditions. The first step would be to incorporate these sensors into an aircraft's bleed air system for a ground tests. NASA's Vehicle Intergraded Propulsion Research (VIPR) intends to simulate a bleed air contamination event by injecting engine oil into the engine of a C-17A and monitoring the gasses that evolve in the bleed air system. Participation in this test would allow the suitability of this class of sensors for bleed air monitoring to be evaluated. If the sensors perform satisfactorily in the VIPR program, then the sensors would be ready for testing on operational aircraft.

## 7. References

- [1] J. D. Anderson, *Introduction to Flight*, 7th ed. New York: McGraw-Hill Education, 2011.
- [2] E. H. Hunt, D. H. Reid, D. R. Space, and F. E. Tilton, “Commercial Airliner Environmental Control System: Engineering Aspects of Cabin Air Quality,” in *Aerospace Medical Association annual meeting*, 1995.
- [3] H. Hinninghofen and P. Enck, “Passenger Well-Being in Airplanes,” *Auton. Neurosci. Nausea Vomiting - Interdiscip. Approach*, vol. 129, no. 1–2, pp. 80–85, Oct. 2006.
- [4] E. H. Hunt and D. R. Space, “The Airplane Cabin Environment,” *TSP*, vol. 3, no. 2, p. 1,000, 1994.
- [5] J. D. Spengler and D. G. Wilson, “Air Quality in Aircraft,” *Proc. Inst. Mech. Eng. Part E J. Process Mech. Eng.*, vol. 217, no. 4, pp. 323–335, 2003.
- [6] “Breathing at High Altitude: The Air Supply of Aircraft Cabins,” *Lufthansa Technik*, 27-Feb-2014. [Online]. Available: <http://www.lufthansa-technik.com/cabin-air-circulation>. [Accessed: 03-Feb-2014].
- [7] R. Haney, “Principal Component Analysis for Enhancement of Infrared Spectra Monitoring,” Auburn University, Auburn, AL, 2011.
- [8] C. Winder and S. Michaelis, “Aircraft Air Quality Malfunction Incidents: Causation, Regulatory, Reporting and Rates,” in *Air Quality in Airplane Cabins and*

- Similar Enclosed Spaces*, vol. 4H, M. Hocking, Ed. Springer Berlin Heidelberg, 2005, pp. 211–228.
- [9] R. Overfelt, B. Jones, S. Loo, H. R, A. Neer, J. Address, X. Yang, A. Zitova, W. Kilpatrick, B. Prorock, J. Fergus, A. Simonian, M. Pook, and M. Anderson, “Sensors and Prognostics to Mitigate Bleed Air Contamination Events - 2012 Progress Report,” National Air Transportation Center of Excellence for Research in the Intermodal Transport Environment, Auburn, AL, RITE-ACER-CoE-2012-TBD, Apr. 2012.
- [10] National Research Council, *The Airliner Cabin Environment and the Health of Passengers and Crew*. Washington DC: National Academies Press, 2002.
- [11] R. Harrison, J. Murawski, E. McNeely, J. Guerriero, and D. Milton, “Exposure to Aircraft Bleed Air Contaminants Among Airline Workers,” Occupational Health Research Consortium in Aviation (OHRCA) and Airliner Cabin Environment Research (ACER) Center of Excellence, Apr. 2009.
- [12] “De-icing Solution Sends Air Crew Members to Hospital,” *CNN*, 24-Dec-2008. [Online]. Available: <http://www.cnn.com/2008/TRAVEL/12/24/holiday.travel/index.html?iref=mpstoryview>. [Accessed: 18-Feb-2014].
- [13] B. Shayne, “Plane with Sick Passengers had Air Contamination Before,” *WCNC*, 20-Jan-2010. [Online]. Available: <http://www.wcnc.com/home/Plane-with-sick-passengers-had-toxic-fume-incident-before-82127832.html>. [Accessed: 18-Feb-2014].
- [14] “Co-Pilot Overcome by Nausea During Cockpit Fume Event,” *Flightglobal*, 02-Feb-2012. [Online]. Available: <http://www.flightglobal.com/news/articles/co-pilot->

- overcome-by-nausea-during-cockpit-fume-event-367718/. [Accessed: 18-Feb-2014].
- [15] *Federal Aviation Regulations 14 C.F.R. § 25.831.*
- [16] *Federal Aviation Regulations 14 C.F.R. § 25.832.*
- [17] M. B. Hocking and D. Hocking, *Air Quality in Airplane Cabins and Similar Enclosed Spaces.* Springer, 2005.
- [18] “Air Carrier Traffic Statistics,” *Research and Innovative Technology Administration: Bureau of Transportation Statistics.* [Online]. Available: [http://apps.bts.gov/xml/air\\_traffic/src/index.xml#CustomizeTable](http://apps.bts.gov/xml/air_traffic/src/index.xml#CustomizeTable). [Accessed: 19-Feb-2014].
- [19] J. T. Murawski and D. S. Supplee, “An Attempt to Characterize the Frequency, Health Impact, and Operational Costs of Oil in the Cabin and Flight Deck Supply Air on US Commercial Aircraft,” *J ASTM Int*, vol. 5, pp. 1–15, 2008.
- [20] “COT Statement on the Review of the Cabin Air Environment, Ill-health in Aircraft Crews and the Possible Relationship to Smoke/Fume Events in Aircraft,” Committee on Toxicology of Chemicals in Food, Consumer Products and the Environment, London, 2007.
- [21] S. Nassauer, “New Worries About Cabin Fume Events,” *Wall Street Journal*, 30-Jul-2009. [Online]. Available: <http://online.wsj.com/news/articles/SB10001424052970204900904574302293012711628>. [Accessed: 19-Feb-2014].
- [22] B. Acker and K. Van Den Wymelenberg, “Demand Control Ventilation: Lessons from the Field- How to Avoid Common Problems.,” *ASHRAE Trans.*, vol. 117, no. 1, pp. 502–508, May 2011.

- [23] K. W. Roth, J. Dieckmann, and J. Brodrick, "Demand Control Ventilation," *ASHRAE J.*, vol. 45, no. 7, pp. 91–92, 2003.
- [24] S. J. Emmerich and A. K. Persily, *State-of-the-Art Review of CO<sub>2</sub> Demand Controlled Ventilation Technology and Application*. DIANE Publishing, 2001.
- [25] American Society of Heating, Refrigerating and Air-Conditioning Engineers, INC, *ASHRE Standard 62.1: Ventilation for Acceptable Indoor Air Quality 2007*. Atlanta, Ga.
- [26] J. W. Jr and L. Weyer, *Practical Guide to Interpretive Near-Infrared Spectroscopy*. Boca Raton, FL: CRC Press, 2007.
- [27] B. C. Smith, *Fundamentals of Fourier Transform Infrared Spectroscopy, Second Edition*, 2nd ed. Boca Raton, FL: CRC Press, 2011.
- [28] L. Robert, "Infrared Spectroscopy Modes of Vibration," 2002. .
- [29] A. Thorne, U. Litzén, and S. Johansson, *Spectrophysics: Principles and Applications*. Springer, 1999.
- [30] "Infrared Sensor Application Note 1: A Background to Gas Sensing by Non-Dispersive Infrared (NDIR)," E2V Technologies, Chelmsford, Essex, UK, 2007.
- [31] S. S. M. Shrestha, "An Experimental Evaluation of HVAC-Grade Carbon Dioxide Sensors - Part 1: Test and Evaluation Procedure," *ASHRAE Trans.*, vol. 115, no. 2, pp. 471–483, Oct. 2009.
- [32] S. S. M. Shrestha, "An Experimental Evaluation of HVAC-Grade Carbon Dioxide Sensors - Part 4: Effects of Ageing on Sensor Performance.," *ASHRAE Trans.*, vol. 116, no. 2, pp. 412–423, Oct. 2010.
- [33] S. Sircar, *Principles of Medical Physiology*. New York: Thieme, 2008.

- [34] *Federal Aviation Regulations 14 C.F.R. § 25.841*. .
- [35] S. J. Emmerich and A. K. Persily, “Literature Review on CO<sub>2</sub>-Based Demand-Controlled Ventilation,” *Trans.-Am. Soc. Heat. Refrig. AIR Cond. Eng.*, vol. 103, pp. 229–243, 1997.
- [36] V. L. Erickson and A. E. Cerpa, “Occupancy Based Demand Response HVAC Control Strategy,” in *Proceedings of the 2nd ACM Workshop on Embedded Sensing Systems for Energy-Efficiency in Building*, Zurich, Switzerland, 2010, pp. 7–12.
- [37] “IR1xxx Series 2, IR2xxx Series 2 Miniature Infrared Gas Sensors for Hazardous Areas and Intrinsic Safety in Mining,” E2V Technologies, Datasheet, 2007.
- [38] “Technical Information for K30 CO<sub>2</sub> Module,” Figaro, Datasheet, 2011.
- [39] “MadIR-D01 CO<sub>2</sub> NDIR Sensor Datasheet,” Madur, Vienna, 2012.
- [40] “Certificate of Calibration Madur madIR-D01 CO<sub>2</sub>,” Madur, Calibration Certificate, Jun. 2012.
- [41] A. Buck, “Steady State and Transient Response Characteristics of Commercial Carbon Monoxide Sensors,” Auburn University, Auburn, 2014.
- [42] S. Ahuja and N. Jespersen, *Modern Instrumental Analysis*, 1st ed., vol. 47. Oxford: Elsevier, 2006.
- [43] E. L. Anderson and R. E. Albert, *Risk Assessment and Indoor Air Quality*. Pages 192-193, CRC Press, 1998.

## Appendix I: Airgas Certificates of Analysis



### CERTIFICATE OF ANALYSIS NITROGEN - RESEARCH

Part Number: NI R300	Reference Number: 55-400020633-1
Cylinder Number: AGA-C141677	Cylinder Volume: 304.0 CF
Laboratory: ASO - Jacksonville - FL	Cylinder Pressure: 2640 PSIG
Analysis Date: Sep 20, 2011	Valve Outlet: 580
Lot Number: 55-400020633-1	

ANALYTICAL RESULTS		
Component	Requested Purity	Certified Concentration
NITROGEN	99.9997 %	99.9997 %
Hydrogen	< 2 PPM	0.1 PPM
THC	< 0.2 PPM	<LDL 0.1 PPM
CO	< 0.5 PPM	<LDL 0.1 PPM
CO2	< 0.5 PPM	<LDL 0.1 PPM
Moisture	< 0.5 PPM	0.1 PPM
Oxygen	< 0.5 PPM	0.1 PPM

Notes:

**Impurities verified against analytical standards traceable to NIST by weight and/or analysis.**

Signature on file

\_\_\_\_\_  
Approved for Release

**Figure A1:** Airgas Certification of 0 ppmv CO<sub>2</sub> Balance N<sub>2</sub>





### CERTIFICATE OF ANALYSIS

Grade of Product: CERTIFIED STANDARD-SPEC

Part Number:	X02NI99C3000023	Reference Number:	42-400078849-1
Cylinder Number:	HO140245	Cylinder Volume:	285.6 CF
Laboratory:	ASO - Theodore Plant - AL	Cylinder Pressure:	2399 PSIG
Analysis Date:	Jul 31, 2012	Valve Outlet:	580
Lot Number:	42-400078849-1		

Product composition verified by direct comparison to calibration standards traceable to N.I.S.T. weights and/or N.I.S.T. Gas Mixture reference materials.

#### ANALYTICAL RESULTS

Component	Requested Concentration	Actual Concentration (Mole %)	Analytical Uncertainty
CARBON DIOXIDE	400.0 PPM	400.6 PPM	+/- 2%
NITROGEN	Balance		

Notes:

Signature on file

Approved for Release

Figure A2: Airgas Certification of 400.6 ppmv CO<sub>2</sub> Balance N<sub>2</sub>



### CERTIFICATE OF ANALYSIS

Grade of Product: CERTIFIED STANDARD-SPEC

Part Number:	X02NI99C30068V6	Reference Number:	42-400078850-1
Cylinder Number:	T441991	Cylinder Volume:	285.6 CF
Laboratory:	ASO - Theodore Plant - AL	Cylinder Pressure:	2399 PSIG
Analysis Date:	Jul 31, 2012	Valve Outlet:	580
Lot Number:	42-400078850-1		

Product composition verified by direct comparison to calibration standards traceable to N.I.S.T. weights and/or N.I.S.T. Gas Mixture reference materials.

#### ANALYTICAL RESULTS

Component	Requested Concentration	Actual Concentration (Mole %)	Analytical Uncertainty
CARBON DIOXIDE	600.0 PPM	591.1 PPM	+/- 2%
NITROGEN	Balance		

Notes:

Signature on file

Approved for Release

Figure A3: Airgas Certification of 591.1 ppmv CO<sub>2</sub> Balance N<sub>2</sub>



### CERTIFICATE OF ANALYSIS

Grade of Product: CERTIFIED STANDARD-SPEC

Part Number:	X02NI99C3003215	Reference Number:	42-400078851-1
Cylinder Number:	SG505274	Cylinder Volume:	285.6 CF
Laboratory:	ASO - Theodore Plant - AL	Cylinder Pressure:	2399 PSIG
Analysis Date:	Jul 31, 2012	Valve Outlet:	580
Lot Number:	42-400078851-1		

Product composition verified by direct comparison to calibration standards traceable to N.I.S.T. weights and/or N.I.S.T. Gas Mixture reference materials.

#### ANALYTICAL RESULTS

Component	Requested Concentration	Actual Concentration (Mole %)	Analytical Uncertainty
CARBON DIOXIDE	800.0 PPM	797.1 PPM	+/- 2%
NITROGEN	Balance		

Notes:

Signature on file

Approved for Release

Figure A4: Airgas Certification of 797.1 ppmv CO<sub>2</sub> Balance N<sub>2</sub>







### CERTIFICATE OF ANALYSIS

Grade of Product: CERTIFIED STANDARD-SPEC

Part Number:	X02NI99C3000004	Reference Number:	42-400078854-1
Cylinder Number:	HO2047189Y	Cylinder Volume:	285.8 CF
Laboratory:	ASO - Theodore Plant - AL	Cylinder Pressure:	2399 PSIG
Analysis Date:	Jul 30, 2012	Valve Outlet:	580
Lot Number:	42-400078854-1		

---

Product composition verified by direct comparison to calibration standards traceable to N.I.S.T. weights and/or N.I.S.T. Gas Mixture reference materials.

#### ANALYTICAL RESULTS

Component	Requested Concentration	Actual Concentration (Mole %)	Analytical Uncertainty
CARBON DIOXIDE	2000 PPM	1889 PPM	+/- 2%
NITROGEN	Balance		

Notes:

Signature on file

---

Approved for Release

**Figure A7:** Airgas Certification of 1889 ppmv CO<sub>2</sub> Balance N<sub>2</sub>



### CERTIFICATE OF ANALYSIS

Grade of Product: CERTIFIED STANDARD-SPEC

Part Number: X04NI78C3HA25V2      Reference Number: 122-124398115-1  
Cylinder Number: ND48338      Cylinder Volume: 250.7 CF  
Laboratory: ASG - Durham - NC      Cylinder Pressure: 2214 PSIG  
Analysis Date: Oct 08, 2013      Valve Outlet: 590  
Lot Number: 122-124398115-1

---

Product composition verified by direct comparison to calibration standards traceable to N.I.S.T. weights and/or N.I.S.T. Gas Mixture reference materials.

#### ANALYTICAL RESULTS

Component	Requested Concentration	Actual Concentration (Mole %)	Analytical Uncertainty
CARBON MONOXIDE	5.000 PPM	5.089 PPM	+/- 5%
CARBON DIOXIDE	400.0 PPM	405.3 PPM	+/- 2%
OXYGEN	21.00 %	21.00 %	+/- 2%
NITROGEN	Balance		

Notes:

Signature on file

---

Approved for Release

**Figure A8:** Airgas Certification of 405.3 ppmv CO<sub>2</sub> Multiple Gas Mixture



### CERTIFICATE OF ANALYSIS

Grade of Product: CERTIFIED STANDARD-SPEC

Part Number: X05NI78C3HA3LS0      Reference Number: 122-124398116-1  
Cylinder Number: ND43427      Cylinder Volume: 250.8 CF  
Laboratory: ASG - Durham - NC      Cylinder Pressure: 2214 PSIG  
Analysis Date: Oct 10, 2013      Valve Outlet: 590  
Lot Number: 122-124398116-1

Product composition verified by direct comparison to calibration standards traceable to N.I.S.T. weights and/or N.I.S.T. Gas Mixture reference materials.

#### ANALYTICAL RESULTS

Component	Requested Concentration	Actual Concentration (Mole %)	Analytical Uncertainty
CARBON MONOXIDE	50.00 PPM	49.73 PPM	+/- 2%
METHANE	500.0 PPM	499.1 PPM	+/- 2%
CARBON DIOXIDE	1500 PPM	1522 PPM	+/- 2%
OXYGEN	21.00 %	21.00 %	+/- 2%
NITROGEN	Balance		

Notes:

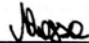
Signature on file

Approved for Release

Figure A9: Airgas Certification of 1522 ppmv CO<sub>2</sub> Multiple Gas Mixture



**Appendix II: Madur madIR-DO1 CO<sub>2</sub> Certificate of Calibration**

INFO		IR Sensor System					
1	Serial number	12060542					
2	Production date (month/year)	06/12					
3	Firmware version	8.7.0					
4	Power supply	15-30V DC or 12-24VAC / 1,1W					
5	Gas	CO <sub>2</sub>					
6	Range	2500ppm					
7	Resolution <1/3 of range	1ppm					
8	Resolution >1/3 of range	10ppm					
9	Averaging time	16s					
10	Analog outputs calibration	Type		Range			
11		U	X	0-10	V		
12		I	X	4-20	mA		
13	Casing	---					
14	MMC Data logger	---					
15	Display	---					
16	Valve	X					
17	Pump	X					
<b>Calibration &amp; settings</b>							
18	Calibration points	Nr	Reference	Signal	Cyclic zeroing	X	
19		1	0ppm	227084	Keep zero after restart	---	
20		2	500ppm	323329			
21		3	1000ppm	376247	Button zero	X	
22		4	1500ppm	414231	Smart zeroing	---	
23		5	2000ppm	443755	"0" gas concentration	400ppm	
24		6	2500ppm	467441	<b>Cycle times</b>		
25		7	---	---	Full cycle time	02:00:00	
26		8	---	---	Ventilation	00:15:00	
27		9	---	---	Measurements	01:45:00	
28		10	---	---	Warming	00:15:00	
29	11	---	---				
30	Analog outputs calibration	U	Ucal min	2V	I	Ical min	4mA
31			C/A min	714		C/A min	614
32			Gas min	0ppm		Gas min	0ppm
33							
34			Ucal max	10V		Ical max	20mA
35			C/A max	3362		C/A max	2763
36		Gas max	2500ppm	Gas max	2500ppm		
<b>Notes</b>							
<b>Final tests</b>							
Test gas		700ppm	Result	697ppm	✓		
Conformity with production card					✓		
Serial number in memory identical with number on sticker					✓		
Serial communication					✓		
Analog outputs calibration					✓		
Propper service settings					✓		
Report storing on MMC card					---		
Display test					---		
Valve test					✓		
Pump test					✓		
Tested by		Signature		Date			
Michał Rossa				18-6-2012			

### Appendix III: Accuracy Evaluation Data

**Table 1A:** Madur madIR-D01 CO<sub>2</sub> Accuracy Results

<b>Actual Concentration (ppmv)</b>	<b>Tests</b>	<b>Average Final Concentration (ppmv)</b>	<b>STDEV Final Concentration (ppmv)</b>	<b>% Error</b>
<b>0</b>	3	5.1	0.0	N/A
<b>400</b>	3	407.8	3.1	+ 1.9
<b>591.1</b>	3	616.9	0.8	+ 4.4
<b>797.1</b>	6	835.3	5.0	+ 4.8
<b>993.7</b>	3	1029.6	4.9	+ 3.6
<b>1501</b>	3	1551.9	0.6	+ 3.4
<b>1889</b>	3	1918.8	4.3	+ 1.6
<b>All Concentrations</b>	<b>24</b>	<b>N/A</b>	<b>N/A</b>	<b>+ 3.3</b>

**Table 2A:** E2V IR11EJ Accuracy Results

<b>Actual Concentration (ppmv)</b>	<b>Tests</b>	<b>Average Final Concentration (ppmv)</b>	<b>STDEV Final Concentration (ppmv)</b>	<b>% Error</b>
<b>0</b>	3	-8.7	0.0	N/A
<b>400</b>	3	369.9	2.0	-7.5
<b>591.1</b>	3	545.6	13.3	-7.7
<b>797.1</b>	3	757.2	2.8	-5.0
<b>993.7</b>	3	940.2	12.3	-5.4
<b>1501</b>	3	1436.6	2.3	-4.3
<b>1889</b>	3	1789.6	20.8	-5.3
<b>All Concentrations</b>	<b>21</b>	<b>N/A</b>	<b>N/A</b>	<b>-5.9</b>

**Table 3A: Figaro K30 Accuracy Results**

<b>Actual Concentration (ppmv)</b>	<b>Tests</b>	<b>Average Final Concentration (ppmv)</b>	<b>STDEV Final Concentration (ppmv)</b>	<b>% Error</b>
<b>0</b>	5	5.1	0.0	N/A
<b>400</b>	5	385.6	0.0	-3.6
<b>591.1</b>	5	583.0	2.6	-1.4
<b>797.1</b>	4	778.9	2.9	-2.3
<b>993.7</b>	5	969.0	5.4	-2.5
<b>1501</b>	5	1471.4	2.9	-2.0
<b>1889</b>	7	1851.6	3.9	-2.0
<b>All Concentrations</b>	<b>36</b>	<b>N/A</b>	<b>N/A</b>	<b>-2.3</b>

#### **Appendix IV: Effect of Flow Rate and Averaging on Response Curves**

One goal of this study was to determine which factors govern the shape of the response curves of the sensors. To determine which factor was rate-limiting, the theoretical concentration of CO<sub>2</sub> in the sensor as a function of time was determined. This curve was then compared to the measured sensor response curve. Additionally, various running averages were applied to the theoretical concentration profile to determine the effect of such an average on the sensor response.

The current concentration of CO<sub>2</sub> in the sensor can be calculated using Equation A1 [43]. This formula is derived from a mass balance and assumes that the gas in the sensor is well mixed. In this equation  $C$ ,  $C_o$ , and  $C_f$  are the current, initial and final concentrations respectively. The time is represented by  $t$ , and the time constant, the exchange rate expressed in seconds per exchange, is represented by  $\tau$ . This constant can be determined using Equation A2 where  $V$  is the volume of the sensor and  $Q$  is the volumetric flow rate.

$$C = (C_f - C_o) \cdot (1 - e^{-t/\tau}) + C_o \quad \text{Eq. A1 [43]}$$

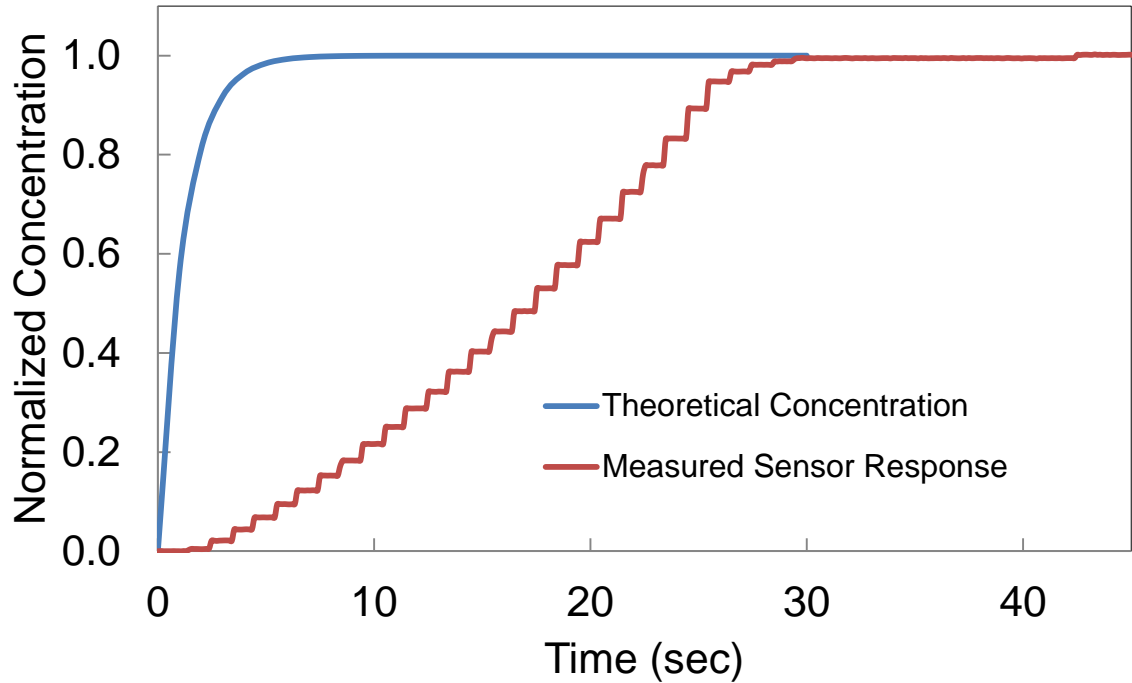
$$\tau = \frac{V}{Q} \quad \text{Eq. A2 [43]}$$

The gas path of the Madur madIR-D01 CO<sub>2</sub> is a cylinder with a diameter of 1.2 cm and a length of 26.7 cm which corresponds to a volume of 30.0 cm<sup>3</sup>. The incorporated

pump provides gas to the sensor at a rate of 1.5 L/min (25 cm<sup>3</sup>/sec). This results in an exchange rate, time constant, of 1.2 sec/exchange. For this sensor, the assumption that the system is well mixed is conservative. If the gasses are not well mixed, the new gas will displace the old gas forcing it out of the gas path. The average velocity of the gas in the sensor was found to be 22.4 cm/sec using Equation A3. In this equation,  $\bar{v}$  is the average velocity, V is the volume of the sensor and A is the cross sectional area of the cylinder. Since the cylinder is 26.7 cm long, if the gas is not mixed, it will reach steady-state in 1.2 sec.

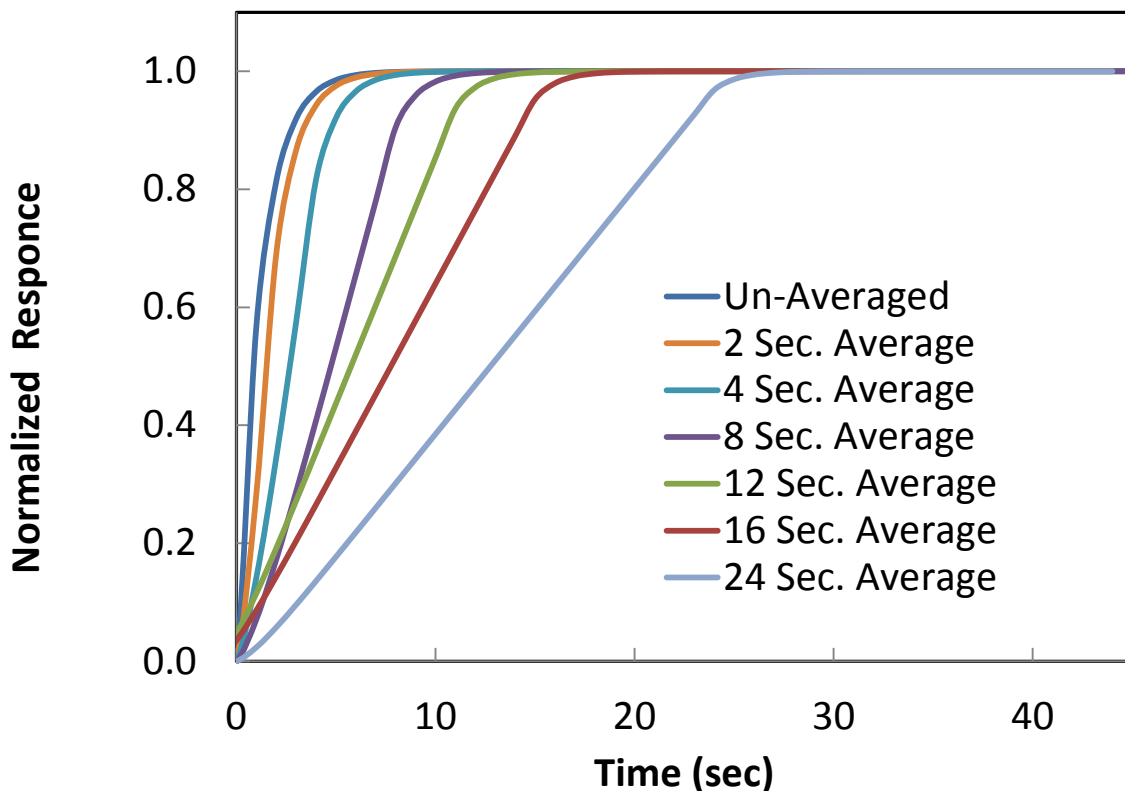
$$\bar{v} = \frac{V}{A} \quad \text{Eq. A3 [43]}$$

Figure A10 compares the measured response of the sensor to the theoretical concentration of the gas present in the sensor. If the response of the sensor was limited by the volumetric flow rate of the gas, the response would follow the theoretical concentration profile. The fact that the response profile of the sensor was longer and did not match the shape of the theoretical concentration profile indicates that other parameters such as the electronics, internal averaging or a combination of the two are dominating the response.



**Figure A10:** Comparison of the measured response of the Madur madIR D01-CO<sub>2</sub> to the theoretical concentration present in the gas path of the sensor.

To evaluate the possible effects of applying a running average, the several one-sided, reverse-looking running averages of various lengths were applied to the theoretical concentration profile (Figure A11). Increasing the interval of the running average causes the concave response to become more convex.



**Figure A11:** Effect of applying various one-sided, reverse-looking running averages to the theoretical concentration profile of the Madur madIR-D01 CO<sub>2</sub>.

The shape of the Madur madIR-DO1 CO<sub>2</sub> response curve is similar to the predicted response if a running average is applied to the theoretical concentration. The response curves from the Madur madIR-D01 CO<sub>2</sub> are not concave, first-order responses functions as one would expect from the concentration predictions. This result indicates that the moving average is dictating the shape of the sensor's response.

Additionally, the application of a sixteen second moving average (as described in the calibration certificate) does not fully account for the longer response time of the sensor compared to the predicted concentration profile. This difference indicates that the

time constant of this system is not determined by the volumetric flow rate, but rather by the electronics or algorithms utilized by the sensor.